

Turing instability and pattern formation on directed networks

J. Ritchie*

Department of Mathematics and Statistics, University of Otago, New Zealand.

May 24, 2022

Abstract

Pattern formation, arising from systems of autonomous reaction-diffusion equations, on networks has become a common topic of study in the scientific literature. In this work we focus primarily on directed networks. Although some work prior has been done to understand how patterns arise on directed networks, these works have restricted their attentions to networks for whom the Laplacian matrix (corresponding to the network) is diagonalizable. Here, we address the question “how does one detect pattern formation if the Laplacian matrix is *not* diagonalizable?” To this end, we find it is useful to also address the related problem of pattern formation arising from systems of reaction-diffusion equations with non-local (global) reaction kinetics. These results are then generalized to include non-autonomous systems as well as temporal networks, i.e., networks whose topology is allowed to change in time.

1 Introduction

Pattern formation occurs when a spatially homogeneous solution is perturbed in a spatially inhomogeneous way leading to finitely many of the spatial modes, corresponding the Laplacian operator, destabilizing. The resulting solution evolves into a spatially inhomogeneous or ‘patterned’ state. This is the so called *Turing instability*. Pattern formation via the Turing mechanism was first introduced by Alan Turing in [1], to provide a mathematical description of morphogenesis. In his work, Turing considered an autonomous system of reaction-diffusion equations. That is, a system of partial differential equations (PDE’s) that do not possess an explicit dependence on their time or space variables. Since then, such systems have become a popular tool for understanding patterning in both biological and chemical systems [2–10].

Although initially introduced for autonomous PDE-systems on continuous manifolds the Turing mechanism has also been applied to networks [11–17]. Recall that a *network* is a collection of nodes, edges (that connect the nodes), and edge weights (that convey

*Email: jritchie@maths.otago.ac.nz

information about “how well” two nodes are connected). Throughout this work we often imagine that one has a known network and the corresponding adjacency matrix A , which contains all of the edge weights. The components of A are A_{ij} , where A_{ij} is the edge-weight connecting node i to node j . If $A_{ij} = 0$ then the two nodes are not connected. Given such a matrix, the corresponding Laplacian can be defined. Here, one studies systems of ordinary differential equations (ODE’s), instead of PDE’s. If the adjacency matrix is symmetric (i.e., $A_{ij} = A_{ji}$) then the underlying graph is referred to as an *undirected network*. Works about pattern forming systems on networks often restrict their attention to undirected networks. This restriction is made for practical purposes as it ensures the Laplacian is symmetric, which in turn means that there exists a coordinate system such that the eigenvectors of the Laplacian define a complete orthonormal basis and hence the autonomous ODE system is symmerizable. In this setting, pattern formation is well understood [11–17]. One particularly interesting property of pattern formation on an undirected networks is that the underlying topology can influence the emergence and suppression of patterning [18, 19].

In some applications one may wish to consider networks for which the adjacency matrix A , is *not* symmetric (i.e., $A_{ij} \neq A_{ji}$). If the adjacency matrix is not symmetric then the underlying graph is referred to as a *directed network*. For this type of graph, edges are allowed to have direction. Directed networks themselves have many applications in the literature [20–23], including pattern formation [24, 25]. Of particular interest to this work is [24]. In their work [24], Asllani et. al. perform a linear instability analysis (which is how pattern forming systems are “detected”) on a class of directed networks. For this they restricted their attentions to the class of directed networks for which the corresponding Laplacian is diagonalizable. In this work here we always refer to networks with this property as *diagonalizable networks*. Similarly, if a network has a corresponding Laplacian matrix that is non-diagonalizable then we say that the network is *non-diagonalizable*. By restricting to diagonalizable networks, Asllani et. al. [24] are able to ensure that there exists a coordinate system such that the eigenvectors of the Laplacian form a complete orthonormal basis. Given this they were able to perform the traditional Turing analysis with only a small adjustment to allow for the now complex eigenvalues. However, the analysis presented in [24] cannot be applied to non-diagonalizable networks. To the best of the authors knowledge there is currently no method for detecting pattern formation on non-diagonalizable networks.

Pattern formation is also known to occur in systems of *non-autonomous* equations. That is ODE (or PDE) systems of reaction diffusion equations that depend explicitly on their time or space coordinates. In order to determine whether or not patterning occurs one must first perform a linear instability analysis. It is tempting to proceed as in the autonomous setting and simply calculate the (now time dependent) eigenvalues of the linearised system. However, it turns out that in the non-autonomous setting one cannot determine instability from the eigenvalues. Indeed there exist counter examples in the literature [26–29]. There have been works addressing this issue [30–32]. Perhaps the most successful of these was presented by Van Gorder in [33] (see also [34]). In [33] Van Gorder uses a second order comparison principal to determine whether or not an instability occurs for a two-species

system of non-autonomous reaction diffusion equations on manifolds. In [35] Van Gorder used his comparison principal to study pattern formation on *undirected temporal networks*, i.e., undirected networks whose topologies are allowed to change in time. To the best of the authors knowledge, *directed temporal networks* have not been studied in the context of pattern formation before.

The approach used by Van Gorder in [33–35] has the drawback that it can only be applied to two-species systems of first order reaction diffusion equations. Moreover, in the case of a continuum, the considered systems are not allowed to depend on their spatial coordinates. These issues were addressed, again by Van Gorder, in [36]. Although networks themselves do not possess any ‘spatial’ coordinates one can think of an analogous scenario in a system of reaction-diffusion equations with *global reaction kinetics*. That is, systems whose reaction kinetics change at each node. Systems (of ODE’s) with global (non-local) reaction kinetics have been studied before on networks [37, 38]. To the best of the authors knowledge, systems with global reaction kinetics have *not* been studied before in the context of pattern formation on directed networks. However, such systems have been considered in the context of pattern formation on *hypergraphs* [38]. Note that global reaction kinetics are not only allowed to change functional form at each node, but they are also allowed depend on the unknowns (that you are solving the ODE’s for) value at any *other* node in the network.

In this work we investigate the following questions: How does one perform a linear instability analysis, to detect pattern formation, in systems of reaction diffusion equations that are: (1) defined over a non-diagonalizable network?; (2) has terms that explicitly depend on time and/or are defined over a directed temporal network?; or (3) have global reaction functions? We address these questions in two parts.

First, we establish a generic method for analysing linear instability in systems of *autonomous* reaction-diffusion equations on static directed networks with (possibly) global reaction kinetics. To do this we *split* the adjacency matrix into its symmetric and anti-symmetric components. We then used the symmetrized adjacency matrix, and its corresponding Laplacian, to find a complete orthonormal basis. This basis is then used to facilitate our linear instability analysis.

Second, we investigate non-autonomous systems of reaction diffusion equations defined over directed temporal networks. For this, we do not perform a basis decomposition. Instead we solve the linearised equations directly.

This paper is outlined as follows: In Section 2 we discuss techniques for detecting patterning on networks. To this end, in Section 2.1, we first give an overview of the standard Turing analysis. In Section 2.2 we then generalize this approach for systems of autonomous reaction-diffusion equations on networks with (or without) global reaction kinetics. Then, in Section 2.3, we discuss how a linear instability analysis could be performed on networks, for systems of *non-autonomous* reaction-diffusion equations. In Section 3 we provide numerical examples of our theory for autonomous reaction-diffusion equations on static networks, and in Section 4 we provide numerical examples of our theory for non-autonomous reaction-diffusion equations on temporal networks. Finally, in Section 5 we summarize our findings.

2 Pattern formation on networks

2.1 Turing instability on undirected networks with autonomous reaction diffusion equations

We begin by first reviewing the Turing instability on undirected networks. To this end we consider the two-species reaction-diffusion system

$$\frac{du_i}{dt} = d_1 \sum_{j=1}^n A_{ij} (u_j - u_i) + f(u_i, v_i), \quad \frac{dv_i}{dt} = d_2 \sum_{j=1}^n A_{ij} (v_j - v_i) + g(u_i, v_i), \quad (2.1)$$

defined over a network, with n nodes, corresponding to the symmetric adjacency matrix A_{ij} . Here d_1 and d_2 are global diffusion rates and the functions f, g are assumed to have continuous derivatives in all arguments. The elements of A measure the connectedness of a pair of nodes i and j , and we assume these can take any values $0 \leq A_{ij} \leq 1$, with a value equal to 0 denoting two nodes which are not connected, while a fractional value strictly between 0 and 1 means that the local rate of diffusion between nodes is less than the maximal rate possible over the network for that species. In this section here we assume that the underlying network is *undirected*, in which case we have that the adjacency matrix is symmetric (i.e., $A_{ij} = A_{ji}$). We now define the Laplacian matrix, L , associated with A in the standard way, i.e., $L_{ij} = \delta_{ij} \sum_{k=1}^n A_{ik} - A_{ij}$, where δ_{kj} denotes the Kronecker delta. For the special case in which the adjacency matrix A is symmetric (i.e., $A_{ij} = A_{ji}$) then the spectral properties of L are well understood: A Laplacian matrix L admits a collection of n distinct eigenvectors, say $\Phi_1, \Phi_2, \dots, \Phi_n \in \mathbb{R}^n$. To each eigenvector Φ_ℓ there exists an eigenvalue $\rho_\ell \geq 0$ such that $L\Phi_\ell = \rho_\ell \Phi_\ell$. Furthermore, we have the eigenvalue $\rho_1 = 0$ and the corresponding eigenvector $\Phi_1 = (1, 1, \dots, 1)^T$. This is the analogue of the Neumann spectral parameter $\rho_0 = 0$ and Neumann eigenfunction $\Psi_0(\mathbf{x}) = 1$ in the case of a continuum domain. However, when the adjacency matrix A is *not* symmetric then the spectral properties are *not* well-understood. In particular, there is no guarantee that the eigenvectors Φ_ℓ form a basis, nor even that there are n of them. We shall return to this point shortly.

We now assume that there exists solutions $u_i = u_\star$ and $v_i = v_\star$ for all $i = 1, 2, \dots, n$ to the algebraic system $f(u_\star, v_\star) = g(u_\star, v_\star) = 0$, which is a constant solution of Eq. (2.1). A diffusive instability, such as the Turing instability, occurs when a perturbation destabilizes such a solution, resulting in a new, spatially inhomogeneous, solution. In order to study instability of such a solution, we consider perturbations of the form $\mathbf{u} = (u_\star, \dots, u_\star)^T + \epsilon \mathbf{U}$ and $\mathbf{v} = (v_\star, \dots, v_\star)^T + \epsilon \mathbf{V}$ where $\mathbf{U} = [U_1, \dots, U_n]^T \in \mathbb{R}^n$ and $\mathbf{V} = [V_1, \dots, V_n]^T \in \mathbb{R}^n$. Putting these expansions into Eq. (2.1) and retaining $\mathcal{O}(\epsilon)$ terms we obtain

$$\frac{d\mathbf{U}}{dt} = d_{11} L\mathbf{U} + d_{12} L\mathbf{V} + J_{11}\mathbf{U} + J_{12}\mathbf{V}, \quad (2.2)$$

$$\frac{d\mathbf{V}}{dt} = d_{21} L\mathbf{U} + d_{22} L\mathbf{V} + J_{21}\mathbf{U} + J_{22}\mathbf{V}, \quad (2.3)$$

where

$$J_{11} = \frac{\partial f}{\partial u}(u_*, v_*), \quad J_{12} = \frac{\partial f}{\partial v}(u_*, v_*), \quad J_{21} = \frac{\partial g}{\partial u}(u_*, v_*), \quad J_{22} = \frac{\partial g}{\partial v}(u_*, v_*). \quad (2.4)$$

In the case of an undirected network the eigenvectors of L form an orthonormal basis i.e., $\Phi_\ell^T \Phi_k = \delta_{\ell k}$. In order to carry forward our analysis we consider the following eigenfunction expansions

$$\mathbf{U} = \sum_{\ell=1}^n A_\ell(t) \Phi_\ell, \quad \mathbf{V} = \sum_{\ell=1}^n B_\ell(t) \Phi_\ell, \quad (2.5)$$

where the A_ℓ and B_ℓ are unknown functions. Then, for each $k = 1, \dots, n$, we obtain the following system of equations

$$\frac{d}{dt} \begin{pmatrix} A_k(t) \\ B_k(t) \end{pmatrix} = M_k \begin{pmatrix} A_k(t) \\ B_k(t) \end{pmatrix}, \quad M_k = J - \rho_k D, \quad (2.6)$$

where

$$J = \begin{pmatrix} J_{11} & J_{12} \\ J_{21} & J_{22} \end{pmatrix}, \quad D = \begin{pmatrix} d_1 & 0 \\ 0 & d_2 \end{pmatrix}. \quad (2.7)$$

It is well known that the stability of the solutions A_k, B_k depends on the eigenvalues of M_k . In particular we have that the solutions A_k, B_k are stable if and only if all of the eigenvalues of M_k have negative real part. If, on the other hand, at least one of the eigenvalues of M_k have positive real part we find that the solutions A_k, B_k are unstable. The eigenvalues of M_k are named λ_k and are determined as solutions of the polynomial equation

$$\lambda_k^2 + (\text{tr}(D)\rho_k - \text{tr}(J))\lambda_k + \det(D)\rho_k^2 - (J_{11}d_2 + J_{22}d_1)\rho_k + \det(J) = 0. \quad (2.8)$$

Using the Ruth-Hurwitz stability criterion we find that $\text{Re}(\lambda_k) < 0$ if and only if

$$\text{tr}(D)\rho_k - \text{tr}(J) > 0, \quad (2.9)$$

$$\det(D)\rho_k^2 - (J_{11}d_2 + J_{22}d_1)\rho_k + \det(J) > 0. \quad (2.10)$$

Recall now that we require u_*, v_* to be stable solutions of. This means that the solutions should be stable in the absence of diffusion. i.e., when $\rho_\ell = 0$. We therefore impose the following restrictions:

$$-\text{tr}(J) > 0, \quad \det(J) > 0. \quad (2.11)$$

These are the standard stability restrictions imposed when studying the Turing instability on undirected graphs. Recall now that, by assumption, we have $\text{tr}(D) > 0$. It follows then that it is *not* possible to violate Eq. (2.9) at any point throughout the evolution. However, it *is* possible to violate Eq. (2.10). This occurs if and only if

$$J_{11}d_2 + J_{22}d_1 > 2\sqrt{\det(D)\det(J)}. \quad (2.12)$$

For such a case, the spatially uniform state is unstable under a perturbation with the ℓ th mode corresponding to ρ_ℓ provided that $0 < \rho_- < \rho_\ell < \rho_+ < \infty$, where

$$\rho_{\pm} = \frac{J_{11}d_2 + J_{22}d_1}{2\det(D)} \pm \frac{\sqrt{(J_{11}d_2 + J_{22}d_1)^2 - 4\det(D)\det(J)}}{2\det(D)}. \quad (2.13)$$

2.2 Generic instability mechanism on static networks

The instability analysis presented in Section 2.1 provides a convenient framework that can be utilized to study instabilities on diagonalizable networks. This approach can even be extended to include more than two unknowns. However, this approach quickly becomes cumbersome as the number of unknowns is increased. Moreover, it is unclear how such an approach can be extended to include non-diagonalizable networks. The goal of this subsection here is to present a method that (1) can be used to determine instability and (2) reduces to the standard Turing analysis in the case of an undirected network with local reaction kinetics. In Section 2.2.1 we present our instability analysis for systems (of ODEs) with m -unknowns defined over an n -node network. This level of generality means that the method we present here is significantly more complicated than the analysis presented in Section 2.1. Here, care should be taken with the notation. In Section 2.2.2 we consider various reductions, of the analysis presented in Section 2.2.1, to less general scenarios. In one of these reductions we demonstrate that, under suitable conditions, the approach we consider here reduces to the standard Turing analysis.

2.2.1 General method

We now consider systems (of ODEs) with m -unknowns defined over an n -node network. As mentioned above, the notation we use here is more complicated than what was presented in Section 2.1. In this subsection all unknowns come equipped with two indices; one Greek and one Latin. Greek indices are used to indicate which unknown is being considered, and therefore run from 1 to m , while lower-case-Latin indices indicate which node the unknown is defined on, and therefore run from 1 to n .

Let us now consider the system

$$\frac{du_{\alpha,i}}{dt} = \sum_{\beta=1}^m d_{\alpha\beta} \sum_{j=1}^n A_{ij} (u_{\beta,j} - u_{\beta,i}) + f_{\alpha,i}(\mathbf{u}), \quad \alpha = 1, \dots, m, \quad i = 1, \dots, n, \quad (2.14)$$

where $\mathbf{u} = (u_{1,1}, \dots, u_{1,n}, u_{2,1}, \dots, u_{2,n}, \dots, u_{m,1}, \dots, u_{m,n})^T$, and

$$f_{\alpha,i}(\mathbf{u}) = f_{\alpha,i}(u_{1,1}, \dots, u_{1,n}, u_{2,1}, \dots, u_{2,n}, \dots, u_{m,1}, \dots, u_{m,n}), \quad (2.15)$$

are global reaction kinetics. If the functions $f_{\alpha,i}(\mathbf{u})$ describe local reaction kinetics then we must have $f_{\alpha,i}(\mathbf{u}) = f_{\alpha}(u_{1,i}, \dots, u_{m,i})$, for some functions $f_{\alpha} : \mathbb{R}^m \rightarrow \mathbb{R}$. For physical applications (of global reaction kinetics) one might expect the functions $f_{\alpha,i}(\mathbf{u})$ to retain their functional form, and vary only in their reaction rates, i.e., $f_{\alpha,i}(\mathbf{u}) = \beta_i f_{\alpha}(\mathbf{u}_i)$ with

$\mathbf{u}_i = (u_{1,i}, \dots, u_{m,i})^T$, and where $\beta_i = \text{constant}$ for each $i = 1, \dots, n$. In this scenario one imagines that reaction rates β_i change at each node to account for physical effects, such as temperature. Although this is the type of example we have in mind when discussing global reaction kinetics we nevertheless present our analysis for more general functions $f_{\alpha,i}(\mathbf{u})$, as it does not significantly change the methodology or indeed the results.

Let us now *split* the adjacency matrix A into its symmetric \tilde{A} and antisymmetric \hat{A} pieces. The components of which are defined as

$$\tilde{A}_{ij} = \frac{1}{2}(A_{ij} + A_{ji}), \quad \hat{A}_{ij} = \frac{1}{2}(A_{ij} - A_{ji}). \quad (2.16)$$

The adjacency matrix A is easily reconstructed as $A = \tilde{A} + \hat{A}$. The matrix \tilde{A}_{ij} can be thought of as the adjacency matrix corresponding to an *undirected* network with n nodes. Taking this view point allows us to define the Laplacian matrix \tilde{L} , associated with \tilde{A} , as $\tilde{L}_{ij} = \delta_{ij} \sum_{k=1}^n \tilde{A}_{ik} - \tilde{A}_{ij}$. Using these definitions we write the reaction-diffusion system Eq. (2.14) as,

$$\frac{du_{\alpha,i}}{dt} = - \sum_{\beta=1}^m d_{\alpha\beta} \sum_{j=1}^n \tilde{L}_{ij} u_{\beta,j} + \hat{f}_{\alpha,i}(\mathbf{u}), \quad \alpha = 1, \dots, m, \quad i = 1, \dots, n, \quad (2.17)$$

where

$$\hat{f}_{\alpha,i}(\mathbf{u}) = \sum_{\beta=1}^m d_{\alpha\beta} \sum_{j=1}^n \hat{A}_{ij} (u_{\beta,j} - u_{\beta,i}) + f_{\alpha,i}(\mathbf{u}). \quad (2.18)$$

From here we see that one may think of the system Eq. (2.14), defined on an directed network, as being equivalent to a problem defined on a *undirected* network, with ‘modified’ reaction kinetics. Similar to what was discussed in Section 2.1, the spectral properties of \tilde{L} are well understood, and hence this is the appropriate setting for our instability analysis.

Suppose now that there exist constants $u_{\alpha,i}^*, \alpha = 1, \dots, m, i = 1, \dots, n$ which are solutions of the algebraic system

$$- \sum_{\beta=1}^m d_{\alpha\beta} \sum_{j=1}^n \tilde{L}_{ij} u_{\beta,j} + \hat{f}_{\alpha,i}(\mathbf{u}) = 0, \quad \alpha = 1, \dots, m, \quad i = 1, \dots, n. \quad (2.19)$$

Then $u_{\alpha,i} = u_{\alpha,i}^*$ is a constant solution of Eq. (2.14). In order to study the stability of such a solution, we consider perturbations of the form

$$u_{\alpha,i} = u_{\alpha,i}^* + \epsilon U_{\alpha,i}, \quad (2.20)$$

where $U_{\alpha,i}, \alpha = 1, \dots, m, i = 1, \dots, n$ and $\epsilon \ll 1$ is a small parameter. Putting these expansions into Eq. (2.17), expanding in ϵ , and retaining $\mathcal{O}(\epsilon)$ terms we obtain the linearised equations

$$\frac{d\mathbf{U}_\alpha}{dt} = - \sum_{\beta=1}^m d_{\alpha\beta} \tilde{L} \mathbf{U}_\beta + \sum_{\beta=1}^m J_{\alpha\beta} \mathbf{U}_\beta, \quad \alpha = 1, \dots, m, \quad (2.21)$$

where $\mathbf{U}_\alpha = (U_{\alpha,1}, \dots, U_{\alpha,n})^T$ and where each $J_{\alpha\beta}, \alpha, \beta = 1, \dots, m$ is an $n \times n$ matrix with entries

$$(J_{\alpha\beta})_{ij} = \frac{\partial \hat{f}_{\alpha,i}}{\partial u_{\beta,j}}(\mathbf{u}^*). \quad (2.22)$$

The eigenvectors of \tilde{L} are Φ_ℓ and the corresponding eigenvalues are σ_ℓ . Let S be the matrix of eigenvectors Φ_ℓ and define

$$\mathbf{v}_\alpha = S \mathbf{U}_\alpha, \quad \alpha = 1, \dots, m. \quad (2.23)$$

Then, one obtains the following evolution equations for \mathbf{v}_α :

$$\frac{d\mathbf{v}_\alpha}{dt} = - \sum_{\beta=1}^m d_{\alpha\beta} P \mathbf{v}_\beta + \sum_{\beta=1}^m \hat{J}_{\alpha\beta} \mathbf{v}_\beta, \quad \alpha = 1, \dots, m, \quad (2.24)$$

where $P = S \tilde{L} S^{-1}$ is the diagonalization of \tilde{L} and $\hat{J}_{\alpha\beta} = S J_{\alpha\beta} S^{-1}$. Before continuing it is useful to briefly discuss why we diagonalise here. In Section 2.1 we not did diagonalise, as the resulting expressions depended only on the eigenvalues (and not the eigenbasis) and as such one does “need” to diagonalise. However, similar to [36], the expression that we obtain here *does* explicitly depend on the eigenbasis. Let us now return to the matrix P . In this coordinate system, the eigenvectors of P are $\mathbf{e}_i, i = 1, \dots, n$ with $(\mathbf{e}_i)_j = \delta_{ij}$. Clearly, the collection of vectors \mathbf{e}_i form an orthonormal basis over \mathbb{R}^n . Now, in order to carry our analysis forward we consider the following eigenvector decomposition:

$$\mathbf{v}_\alpha = \sum_{\ell=1}^n B_{\alpha,\ell} \mathbf{e}_\ell, \quad \alpha = 1, \dots, m, \quad (2.25)$$

where $B_{\alpha,\ell}, \alpha = 1, \dots, m, \ell = 1, \dots, n$ are unknown functions of time. The resulting system of equations is

$$\sum_{\ell=1}^n \left(\frac{dB_{\alpha,\ell}}{dt} + \sigma_\ell \sum_{\beta=1}^m d_{\alpha\beta} B_{\alpha,\ell} \right) \mathbf{e}_\ell = \sum_{\ell=1}^n \sum_{\beta=1}^m \hat{J}_{\alpha\beta} B_{\beta,\ell} \mathbf{e}_\ell, \quad \alpha = 1, \dots, m. \quad (2.26)$$

To make further progress we note that, for each $\alpha, \beta = 1, \dots, m$ and $\ell = 1, \dots, n$ the quantity $\hat{J}_{\alpha\beta} \mathbf{e}_\ell$ is a vector and can therefore be written as

$$\hat{J}_{\alpha\beta} \mathbf{e}_\ell = \sum_{r=1}^n \gamma_{r,\ell,\alpha,\beta} \mathbf{e}_r, \quad (2.27)$$

where, for each $\alpha, \beta = 1, \dots, m$ and $k, \ell = 1, \dots, n$, we have $\gamma_{k,\ell,\alpha,\beta} = \mathbf{e}_k^T \hat{J}_{\alpha\beta} \mathbf{e}_\ell$. Moreover, for $k, \ell = 1, \dots, n$ we define the $m \times m$ matrices $\Gamma_{k,\ell}$ and D as $(\Gamma_{k,\ell})_{\alpha\beta} = \gamma_{k,\ell,\alpha,\beta}$ and $(D)_{\alpha\beta} = d_{\alpha\beta}$. Returning now to Eqs. (2.26) we multiply by \mathbf{e}_k^T , and sum over k , to obtain

$$\frac{d\mathbf{B}_k}{dt} + \sigma_k D \mathbf{B}_k = \sum_{\ell=1}^n \Gamma_{k,\ell} \mathbf{B}_\ell, \quad k = 1, \dots, n \quad (2.28)$$

where we have introduced the notation $\mathbf{B}_k = (B_{1,k}, \dots, B_{m,k})^T$. Notice that, unlike in Section 2.1, the modes have *not* decoupled. Because of this it is, in general, not possible to derive an explicit inequality that determines stability.

In order to understand when an instability occurs, we now define $\mathbf{w} = (\mathbf{B}_1, \dots, \mathbf{B}_n)^T$ so that Eqs. (2.28) can be written in matrix form as

$$\frac{d\mathbf{w}}{dt} = M\mathbf{w}, \quad (2.29)$$

where M is an $(nm) \times (nm)$ constant matrix with each $n \times n$ element $M_{k\ell}$ an $m \times m$ matrix of the form $M_{k\ell} = -D\sigma_k\delta_{k\ell} + \Gamma_{k,\ell}$.

In order to understand whether or not an instability occurs one must study the eigenvalues of M . Throughout this work we often represent the eigenvalues of M as λ_ℓ . If one of the eigenvalues has positive real part then an instability (such as the Turing instability) occurs, i.e., the steady state solution $u_{\alpha,i}^*$ is unstable if $\max_\ell \text{Re}(\lambda_\ell) > 0$. This is our instability criterion. Although it is not, in general, possible to find the eigenvalues of M explicitly, we note that they are easily calculated *numerically* using programs such as *Python*, *Matlab*, or *Mathematica*.

2.2.2 Reductions

We now consider two special cases of Section 2.2.1. The goal here is to show that the analysis presented in Section 2.2.1 reduces to the standard Turing analysis (see Section 2.2), under the appropriate assumptions.

Reduction for local reaction kinetics. Suppose now that the reaction kinetics in Eq. (2.14) are *local*, i.e., $f_{\alpha,i}(\mathbf{u}) = f_\alpha(\mathbf{u}_i)$ for all $\alpha = 1, \dots, m$ and $i = 1, \dots, n$ where $\mathbf{u}_i = (u_{1,i}, \dots, u_{m,i})^T$. In this special case we find that the modified reaction kinetics (defined in Eq. (2.18)) are

$$\hat{f}_{\alpha,i}(\mathbf{u}) = \sum_{\beta=1}^m d_{\alpha\beta} \sum_{j=1}^n \hat{A}_{ij} (u_{\beta,j} - u_{\beta,i}) + f_\alpha(\mathbf{u}_i). \quad (2.30)$$

Moreover, we find that the matrices $J_{\alpha\beta}$ are

$$(J_{\alpha\beta})_{ij} = -d_{\alpha\beta} \hat{L}_{ij} + \mathcal{J}_{\alpha\beta} \delta_{ij}, \quad (2.31)$$

where we have defined \hat{L}_{ij} as $\hat{L}_{ij} = \delta_{ij} \sum_{k=1}^n \hat{A}_{ik} - \hat{A}_{ij}$, and the *constants* $\mathcal{J}_{\alpha\beta}$ (for $\alpha, \beta = 1, \dots, m$) as

$$\mathcal{J}_{\alpha\beta} = \frac{\partial \hat{f}_\alpha}{\partial u_{\beta,i}}(\mathbf{u}^*). \quad (2.32)$$

Moreover, we find that $\hat{J}_{\alpha\beta} = -d_{\alpha\beta}S\hat{L}S^{-1} + \mathcal{J}_{\alpha\beta}I_n$, where I_n is the $n \times n$ identity matrix. Recall that S is the matrix of eigenvectors of the symmetrised Laplacian \tilde{L} . Using this particular form $\hat{J}_{\alpha\beta}$ we calculate the constants $\gamma_{k,\ell,\alpha,\beta}$ as

$$\gamma_{k,\ell,\alpha,\beta} = -d_{\alpha\beta}\Omega_{k\ell} + \mathcal{J}_{\alpha\beta}\delta_{k\ell}, \quad \Omega_{k\ell} = \mathbf{e}_k^T S \hat{L} S^{-1} \mathbf{e}_\ell. \quad (2.33)$$

The $m \times m$ matrices $\Gamma_{k,\ell}$ are therefore $\Gamma_{k,\ell} = \Omega_{k\ell}D_{\alpha\beta} + \mathcal{J}\delta_{k\ell}$, where D and \mathcal{J} are $m \times m$ matrices with entries $d_{\alpha\beta}$ and $\mathcal{J}_{\alpha\beta}$, respectively. Finally, we find that the $(nm) \times (nm)$ matrix M (see Eq. (2.29)) has elements $M_{k\ell} = (-D\sigma_k + \mathcal{J})\delta_{k\ell} - D\Omega_{k\ell}$.

Reduction to the standard Turing analysis. Suppose now that, in addition to local reaction kinetics, the adjacency matrix A_{ij} represents an *undirected* network (so that $A_{ij} = A_{ji}$). Then, one expects that the analysis presented in Section 2.1 is applicable (although now one has m equations, instead of just two). To demonstrate this we use the results of the previous paragraph with $\hat{A}_{ij} = \hat{L}_{ij} = \Omega_{ij} = 0$. In this case we find that M is a block diagonal matrix with each $n \times n$ block taking the form, $M_{kk} = (-D\sigma_k + \mathcal{J})\delta_{k\ell}$. One can therefore determine the eigenvalues of M by calculating the eigenvalues of M_{kk} for each $k = 1, \dots, n$.

This is equivalent to the standard Turing analysis. To explicitly demonstrate this we now set $m = 2$. Then,

$$M_{kk} = \begin{pmatrix} J_{11} & J_{12} \\ J_{21} & J_{22} \end{pmatrix} - \sigma_k \begin{pmatrix} d_{11} & d_{12} \\ d_{21} & d_{22} \end{pmatrix}. \quad (2.34)$$

Compare this to Eq. (2.6) and note that the eigenvalues of L and \tilde{L} are equal (i.e., $\sigma_\ell = \rho_\ell$) since $A_{ij} = \tilde{A}_{ij}$ (and hence $L_{ij} = \tilde{L}_{ij}$). This suggests that our approach here is one possible generalisation of the standard Turing analysis.

2.3 Linear instability analysis on temporal networks

Now that we are now able to detect instability for a general class of autonomous reaction-diffusion equations, it is natural to wonder to what extent these results can be extended to include *non-autonomous* systems. The purpose of this subsection is to address exactly this issue. To this end, we now consider the following system of non-autonomous reaction-diffusion equations:

$$\frac{du_{\alpha,i}}{dt} = \sum_{\beta=1}^m d_{\alpha\beta}(t) \sum_{j=1}^n A_{ij}(t) (u_{\beta,j} - u_{\beta,i}) + f_{\alpha,i}(\mathbf{u}, t), \quad \alpha = 1, \dots, m, \quad i = 1, \dots, n. \quad (2.35)$$

Note that Eq. (2.35) corresponds to a static network if and only if $dA_{ij}/dt = 0$ for all $i, j = 1, \dots, n$. Suppose now that there exists a solution $u_{\alpha,i}^*(t)$, $\alpha = 1, \dots, m$, $i = 1, \dots, n$ of Eq. (2.35). Notice here that, unlike in Section 2.2, we do not require that the background solution $u_{\alpha,i}^*(t)$ is constant in time. Then we consider perturbations of the form $u_{\alpha,i} =$

$u_{\alpha,i}^* + \epsilon U_{\alpha,i}$, where $U_{\alpha,i}, \alpha = 1, \dots, m, i = 1, \dots, n$ and $\epsilon \ll 1$ is a small parameter. Putting these expansions into Eq. (2.35) and retaining $\mathcal{O}(\epsilon)$ terms we obtain

$$\frac{dU_{\alpha,i}}{dt} = \sum_{\beta=1}^m \sum_{j=1}^n (d_{\alpha\beta}(t) A_{ij}(t) (U_{\beta,j} - U_{\beta,i}) + (J_{\alpha\beta})_{ij}(t) U_{\beta,j}), \quad \alpha = 1, \dots, m, \quad i = 1, \dots, n, \quad (2.36)$$

where $J_{\alpha\beta}, \alpha, \beta = 1, \dots, m$ is defined as in Eq. (2.22). From here one could proceed in much the same way as in Section 2.2. i.e., by symmetrising the adjacency matrix and performing an eigenbasis decomposition. The calculations that follow are near identical to what was done in Section 2.2, with the only significant difference coming from a modified definition of $\gamma_{k,\ell,\alpha,\beta}$. In this temporal setting, for $k, \ell = 1, \dots, n$, and $\alpha, \beta = 1, \dots, m$, one defines the functions $\gamma_{k,\ell,\alpha,\beta} : \mathbb{R} \rightarrow \mathbb{R}$ as

$$\gamma_{k,\ell,\alpha,\beta} = \mathbf{e}_k^T \left(\hat{J}_{\alpha\beta} - S \frac{d}{dt} S^{-1} \delta_{\alpha\beta} \right) \mathbf{e}_\ell, \quad k, \ell = 1, \dots, n \quad \alpha, \beta = 1, \dots, m. \quad (2.37)$$

Doing this allows one to once again obtain a system of the form Eq. (2.29). From here one could proceed as in [36] by numerically solving the resulting equations, or some subsystem. There are some benefits to this approach. As one can easily define a subsystem i.e., a reduced system of ODE's also of the form Eq. (2.29) where the 'reduced M ' has a lower dimension than the original system. However, this approach is not without its own drawbacks. For example, in order to calculate $\gamma_{k,\ell,\alpha,\beta}$ one must first find S and S^{-1} . Recall here that S is the matrix of eigenvectors of the symmetrized Laplacian \tilde{L} . Although numerically calculating S (and S^{-1}) is easily done on a computer in the case of a static network (i.e., networks that satisfy $dA_{ij}/dt = 0$ for all $i, j = 1, \dots, n$), this becomes more complicated for a dynamical network as, in addition to S and S^{-1} , one must now also numerically calculate $\frac{d}{dt} S^{-1}$. For this, one might consider using a central finite differencing approximation. However, care should be taken here as approximating the derivative in this way could be a significant source of numerical error, particularly if S^{-1} changes rapidly. For this reason we do not consider this approach here. Instead we opt to numerically solve the linearized system Eq. (2.36), without any further reductions. One may ask "why not numerically solve the non-linear system Eq. (2.35) instead?" This is a reasonable question as, in either case, one must numerically solve nm ODE's. However, it is worth noting that it is less computationally expensive to solve linear equations, than it is to solve non-linear ones.

3 Numerical examples of pattern formation on static directed networks

We now provide numerical examples of the theory presented in Section 2.2. In particular we numerically solve equations of the form Eq. (2.14). The goal of this section is twofold: On the one hand, we provide examples of pattern formation on static non-diagonalizable

networks. On the other hand, we provide examples of pattern formation (on static networks) arising from global reaction kinetics. In this section we consider only two types of networks. Many of the results can of course be applied to other types of networks. However, we find that the ones considered here are sufficient to demonstrate the different aspects of our theory.

3.1 Numerical methods

We numerically solve equations of the form Eq. (2.14), using the Mathematica function *NDSolve*¹, which has an absolute error tolerance of 10^{-8} . Moreover, suppose that $u_{\alpha,i}^*$ for $\alpha = 1, \dots, m$ and $i = 1, \dots, n$ is a constant steady-state solution of Eq. (2.14). Then, for initial data, we pick $u_{\alpha,i}(0) = u_{\alpha,i}^* + \xi_{\alpha,i}$, where $\xi_{\alpha,i}$ is a random real number. Here, we calculate $\xi_{\alpha,i}$ using the Mathematica function² *RandomReal*[1].

3.2 A simple example of our instability criterion

To demonstrate the theory outlined in Section 2.2, we first consider systems with *local reaction kinetics*. The goal of this subsection here is to give an explicit example of our instability criterion on a non-diagonalizable network. For this we study equations of the form

$$\frac{du_i}{dt} = \frac{1}{50} \sum_{j=1}^n A_{ij} (u_j - u_i) + \frac{1}{10} - u_i + u_i^2 v_i, \quad (3.1)$$

$$\frac{dv_i}{dt} = \sum_{j=1}^n A_{ij} (v_j - v_i) + 1 - u_i^2 v_i, \quad (3.2)$$

for $n = 4$, where A is given below. It is worth noting that the reaction kinetics we have chosen here are the Schnakenberg kinetics. A locally stable steady state is given by $(u_i, v_i) = (u^*, v^*)$ with $u^* = 11/10$ and $v^* = 100/121$.

Let us now consider a 4-node directed network with the following adjacency matrix

$$A = \frac{1}{2} \begin{pmatrix} 0 & 2 & 2 & 2 \\ 2 & 0 & 1 & 0 \\ 2 & 1 & 0 & 0 \\ 2 & 2 & 0 & 0 \end{pmatrix} \implies L = -\frac{1}{2} \begin{pmatrix} -6 & 2 & 2 & 2 \\ 2 & -3 & 1 & 0 \\ 2 & 1 & -3 & 0 \\ 2 & 2 & 0 & -4 \end{pmatrix}, \quad (3.3)$$

where L is the Laplacian matrix corresponding to A . This network is directed since $A_{24} \neq A_{42}$. The eigenvectors corresponding to the Laplacian L are $\Phi_1 = (1, 1, 1, 1)^T$, $\Phi_2 = (0, 0, 0, 0)^T$, $\Phi_3 = (1/3, 1/3, 1/3, 1)^T$ and $\Phi_4 = (-3, 1, 1, 1)^T$ and the corresponding eigenvalues are $\rho_1 = 0$, $\rho_2 = 2$, $\rho_3 = 2$, and $\rho_4 = 4$. Here we see that the eigenvectors clearly do not form a basis and hence the Laplacian L is non-diagonalizable. Thus, in order to detect

¹See <https://reference.wolfram.com/language/ref/NDSolve.html>

²see <https://reference.wolfram.com/language/ref/RandomReal.html>

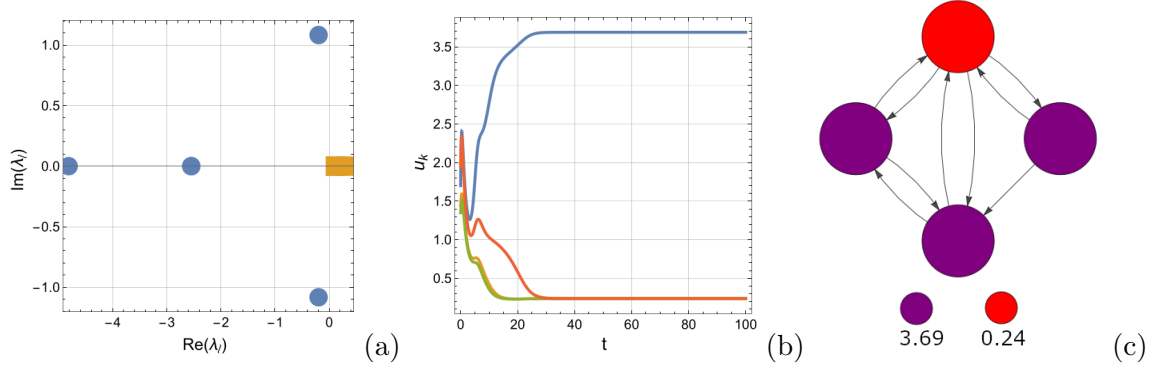


Figure 1: Patterning corresponding to the adjacency matrix Eq. (3.3). In (a) we give the eigenvalues of the matrix M . In (b) we show the behaviour of the function u , for each of the nodes. Finally, in (c) we give the pattern for the function u at $t = 100$.

a Turning instability one must use the theory presented by us in Section 2.2. To this end we now calculate the symmetrised adjacency matrix, and its associated Laplacian, as

$$\tilde{A} = \frac{1}{2} \begin{pmatrix} 0 & 2 & 2 & 2 \\ 2 & 0 & 1 & 1 \\ 2 & 1 & 0 & 0 \\ 2 & 1 & 0 & 0 \end{pmatrix} \Rightarrow \tilde{L} = -\frac{1}{2} \begin{pmatrix} -6 & 2 & 2 & 2 \\ 2 & -4 & 1 & 1 \\ 2 & 1 & -3 & 0 \\ 2 & 1 & 0 & -3 \end{pmatrix}. \quad (3.4)$$

The eigenvalues of \tilde{L} are $\sigma_1 = 0, \sigma_2 = 3/2, \sigma_3 = 5/2$, and $\sigma_4 = 4$. From here it is straightforward to calculate the matrix M as is described in Section 2.2. In doing so we obtain

$$M = \begin{pmatrix} 0.738 & 1.21 & -0.01 & 0 & -0.01 & 0 & 0 & 0 \\ -1.81 & -5.21 & 0 & -0.5 & 0 & -0.5 & 0 & 0 \\ 0 & 0 & 0.773 & 1.21 & 0.005 & 0 & 0 & 0 \\ 0 & 0 & -1.818 & -3.46 & 0 & 0.25 & 0 & 0 \\ 0 & 0 & -0.005 & 0 & 0.783 & 1.21 & 0 & 0 \\ 0 & 0 & 0 & -0.25 & -1.818 & -2.96 & 0 & 0 \\ 0 & 0 & -0.01 & 0 & -0.01 & 0 & 0.818 & 1.21 \\ 0 & 0 & 0 & -0.5 & 0 & -0.5 & 1.818 & -1.21 \end{pmatrix}. \quad (3.5)$$

The corresponding eigenvalues are $\lambda_1 = -4.81, \lambda_2 = \lambda_3 = -2.58, \lambda_4 = -0.19 + 1.08i, \lambda_5 = -0.19 - 1.08i, \lambda_6 = 0.34, \lambda_7 = \lambda_8 = 0.12$. Observe carefully that there are *three* eigenvalues with positive real part, with $\max_{\ell} \text{Re}(\lambda_{\ell}) = 0.34 > 0$. We therefore expect this network to give rise to a patterned state. The numerical results for this case are shown in Fig. 1. In Fig. 1(a) we give the eigenvalues of the matrix M . The blue dots shows eigenvalues with negative real part and the orange squares show eigenvalues with positive real part. In Fig. 1(b) we show each u_i as a function of time t . Here we see that a stable pattern forms at around $t \approx 45$. In Fig. 1(c) we show the pattern, emergent at $t = 100$, corresponding to the values of u_i . Similar plots can be made for v_i .

3.3 Influence of directed edges on Turing pattern formation

For our next examples we once again consider Eqs. (3.1) and (3.2). However, this time we pick $n = 16$ and set the adjacency matrix as

$$A_{ij} = \begin{cases} 1/2 & \text{if } i - j = 1 \text{ or } i - j = 15, \\ a_1 & \text{if } j - i = 1 \text{ or } j - i = 15, \\ 0 & \text{if } i - j = 0 \\ a_2 & \text{otherwise,} \end{cases} \quad (3.6)$$

for $1 \leq i, j \leq 16$. Here, a_1 and a_2 are freely specifiable constants with $a_1, a_2 \in [0, 1]$. Note that A_{ij} is symmetric if and only if $a_1 = 1/2$. Moreover, A_{ij} describes a complete graph if $a_1, a_2 \neq 0$ and a cycle graph if $a_2 = 0$. To ease much of the upcoming discussions we now briefly introduce some terminology. In the special case $a_1 = 0$ and $a_2 \neq 0$, we refer to the network as a *complete cycle graph*. For these particular parameter choices each node is connected to all other nodes, excluding its left most neighbour. This network is of course not a complete network. nevertheless we find this terminology useful for our purposes here. Similarly, in the special case $a_1 = a_2 = 0$, we refer to the network as an *incomplete cycle graph*. In setting each node is connected (via a directed edge) only to its left most neighbour. It is worth noting that an incomplete cycle graph, regardless of the number of nodes, is a non-diagonalizable network.

We now consider some numerical examples of patterning on networks described by Eq. (3.6). Here, we focus primarily on what effect the parameters a_1 and a_2 have on the emergence of patterning. To this end, we first consider the choices $a_1 = 1/2$ and $a_2 = 0$. The numerical results corresponding to these choices are shown in the top row of Fig. 2 (plots (a)–(c)). In this case the adjacency matrix is symmetric and hence the standard Turing analysis (presented in Section 2.1) can be applied. In Fig. 2(a) we give the eigenvalues of the matrix M . As with the previous example, the blue dots shows eigenvalues with negative real part and the orange squares show eigenvalues with positive real part. We find that there are three (non-distinct) eigenvalues with negative real part. In particular, we find that $\text{Re}(\lambda_\ell) = 0.12 > 0$ and hence we detect an instability. In Fig. 2(b) we show u_i as a function of time t for each $i = 1, \dots, 16$. Here see that a stable pattern forms at around $t \approx 40$. In Fig. 2(c) we show the pattern corresponding to the values of u_i at $t = 100$.

Conversely, in the second row of Fig. 2 (plots (d)–(f)), we show the results corresponding to the parameter choices $a_1 = a_2 = 0$. In this setting the underlying network is an incomplete cycle graph. We find that all of the eigenvalues (of M) have negative real part (with $\text{Re}(\lambda_\ell) = -0.2 < 0$) and, as such, are linearly stable. This is clearly seen in Fig. 2(e). The values of u_i , for $i = 1, \dots, 16$, at $t = 100$ are shown in Fig. 2(f) on the incomplete cycle graph. It is interesting to note here that the presence of directed edges, at least in this particular example, have the effect of suppressing the formation of patterning. This shows that, as with the undirected networks, the underlying topology (of the network) plays an important role in the generation of a pattern. In particular, we see that the presence of directed edges can actually *stabilize* the background solution.

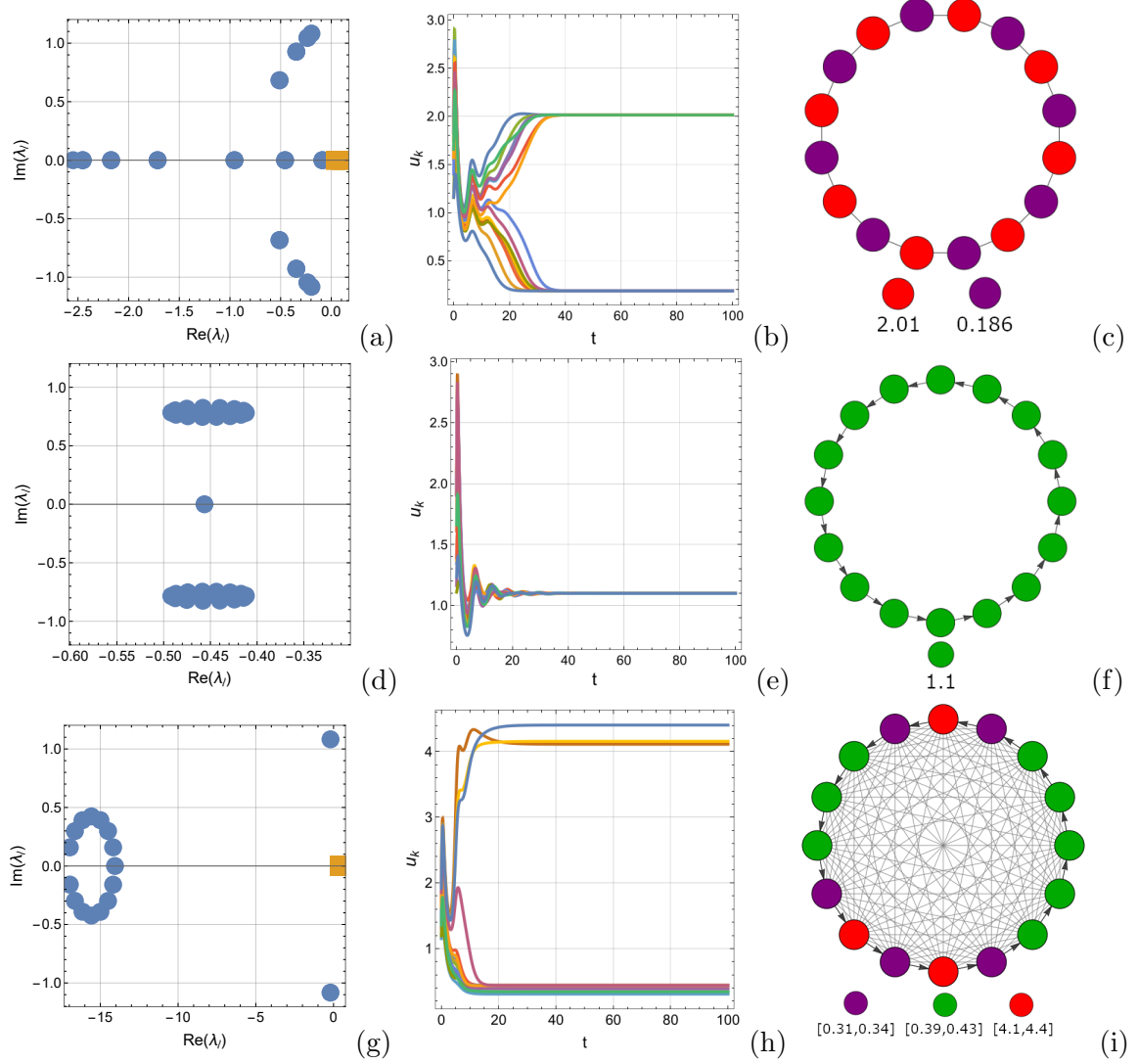


Figure 2: Patterning corresponding to the adjacency matrix Eq. (3.6). The first row (plots (a)–(c)) shows the numerical results corresponding to setting $a_1 = 1/2$ and $a_2 = 0$. The second row (plots (d)–(f)) shows the numerical results corresponding to setting $a_1 = a_2 = 0$, and the third row (plots (g)–(i)) shows the numerical results corresponding to setting $a_1 = 0$ and $a_2 = 1$. Plots (a),(d) and (g) give the eigenvalues of the matrix M for each of the considered cases. Similarly, plots (b),(e), and (h) show the function u . Lastly, plots (c),(f) and (i) show the pattern corresponding to the function u at $t = 100$.

Of course, the presence of directed edges, does not *always* suppress the emergence of a pattern. To see this we consider a complete cycle graph (described by the choices $a_1 = 0$ and $a_2 = 1$). The numerical results, corresponding to these parameter choices, are given in the last row of Fig. 2 (plots (g)–(i)). In Fig. 2(g) we show the eigenvalues of the matrix M . In this case we find that there are 8 distinct eigenvalues with positive real part. In particular, we find that $\text{Re}(\lambda_\ell) = 0.41 > 0$ and hence we detect an instability. In Fig. 2(h) we plot the functions u_i , for $i = 1, \dots, n$, as a function of time. Here we find that a stable pattern emerges at around $t \approx 25$. The resulting pattern, corresponding to $u_i, i = 1, \dots, 16$ at $t = 100$, is shown in Fig. 2(i).

3.4 Pattern formation from hyperbolic reaction-diffusion equations

Having now seen some examples of patterning on static networks for two-species system of reaction-diffusion equations, it is interesting to now consider an example of patterning (on a static network) with *more* than two equations. Recall that Section 2.2 allows for arbitrarily (but finitely) many equations. To this end we consider the following system:

$$\frac{d^2 u_i}{dt^2} + \frac{du_i}{dt} = 3 \sum_{j=1}^{10} A_{ij} (u_j - u_i) + 5 - 10u_i + u_i^2 v_i, \quad (3.7)$$

$$\frac{d^2 v_i}{dt^2} + \frac{dv_i}{dt} = \sum_{j=1}^{10} A_{ij} (v_j - v_i) + 9u_i - u_i^2 v_i, \quad (3.8)$$

where

$$A_{ij} = \begin{cases} 1 & \text{if } i = 1 \text{ and } j \neq 1 \text{ or } j = 1 \text{ and } i \neq 1, \\ 1/2 & \text{if } i = 2 \text{ and } j = 3 \text{ or } i = 3 \text{ and } j = 2, \\ 1 & \text{if } i = 4 \text{ and } j = 2, \\ 0 & \text{otherwise,} \end{cases} \quad (3.9)$$

for $1 \leq i, j \leq 10$. This adjacency matrix describes a modified star graph (with 10 nodes) where, in addition to the standard star graph connections, nodes two and three are connected by an undirected edge and node four is connected to node two via a directed edge. Although these modifications (to the star graph) may seem like a small change, it turns out that this adjacency matrix describes a non-diagonalizable network. Observe carefully that, written in this way, Eqs. (3.7) and (3.7) form a system of *hyperbolic reaction-diffusion* equations. Systems of this type have been investigated before in the context of pattern formation in [39–41]. Moreover, we note that we have chosen to use the Brusselator reaction-kinetics which has a locally stable steady state is given by $(u_i, v_i) = (u^*, v^*)$ with $u^* = 5$ and $v^* = 9/5$.

In order to use the theory presented in Section 2.2 we now define $u_{1,i} = u_i, u_{2,i} =$

$du_i/dt, u_{3,i} = v_i$ and $u_{4,i} = dv_i/dt$. The resulting evolution equations for $u_{2,i}$ and $u_{4,i}$ are

$$\frac{du_{2,i}}{dt} + u_{2,i} = 3 \sum_{j=1}^n A_{ij} (u_{1,j} - u_{1,i}) + 5 - 10u_{1,i} + u_{1,i}^2 u_{3,i} \quad (3.10)$$

$$\frac{du_{4,i}}{dt} + u_{4,i} = \sum_{j=1}^n A_{ij} (u_{3,j} - u_{3,i}) + 9u_{1,i} - u_{1,i}^2 u_{3,i}. \quad (3.11)$$

Together Eqs. (3.10)–(3.11) take the form of Eqs. (2.14) with $m = 4$, $d_{21} = 3$, $d_{43} = 1$ and $d_{\alpha\beta} = 0$ otherwise. Moreover, the reaction kinetics are

$$\begin{aligned} f_{1,i}(\mathbf{u}) &= u_{2,i}, & f_{2,i}(\mathbf{u}) &= 5 - 10u_{1,i} + u_{1,i}^2 u_{3,i} - u_{2,i}, \\ f_{3,i}(\mathbf{u}) &= u_{4,i}, & f_{4,i}(\mathbf{u}) &= 9u_{1,i} - u_{1,i}^2 u_{3,i} - u_{4,i}. \end{aligned}$$

A numerical example, of pattern formation resulting from Eqs. (3.10)–(3.11), is shown in Fig. 3. In Fig. 3(a) we give the eigenvalues of the matrix M , corresponding to Eq. (3.9). Here, we see that there are four eigenvalues (two conjugate pairs) with positive real part. In particular we find that $\text{Re}(\lambda_\ell) = 0.74 > 0$, and hence we detect an instability. Interestingly, all of these eigenvalues also have a non-zero imaginary part. Recall that if the dominant eigenvalue (i.e., the eigenvalue with the largest real part) has a non-zero imaginary part then it is indicative of the *Turing-wave instability* (also often just called a *wave-instability*) [42]. This means that we do not expect the unknowns to approach a time independent steady state. This behaviour is confirmed in Fig. 3(b)–(f), where we see that the functions u_i ($u_{1,i}$) *does not* become constant in time. In Fig. 3 we see that the values of u_i at each node naturally separate into five groups, each of which oscillate with the same frequency and amplitude. The plots for each of these groups are given in Fig. 3(b)–(f). In Fig. 3(g) we show the patterning resulting from u_i with $i = 1, \dots, n$ at different times.

3.5 Pattern formation with global reaction kinetics

In addition to being able to identify instabilities for non-diagonalizable networks, the theory outlined in Section 2.2 can be applied when studying systems with *global* reaction kinetics. In such a system the reaction kinetics can not only differ for each unknown but also at each node. The goal of this subsection here is to investigate an example of such system. For this, we consider the following equations

$$\frac{du_i}{dt} = \frac{2}{100} \sum_{j=1}^n A_{ij} (u_j - u_i) + \beta_i \left(\frac{1}{10} - u_i + u_i^2 v_i \right), \quad (3.12)$$

$$\frac{dv_i}{dt} = \sum_{j=1}^n A_{ij} (v_j - v_i) + \beta_i (1 - u_i^2 v_i), \quad (3.13)$$

where $\beta_i, i = 1, \dots, n$ are freely specifiable constants. This particular choice (of global reaction kinetics) the reaction kinetics themselves maintain their function form but allow

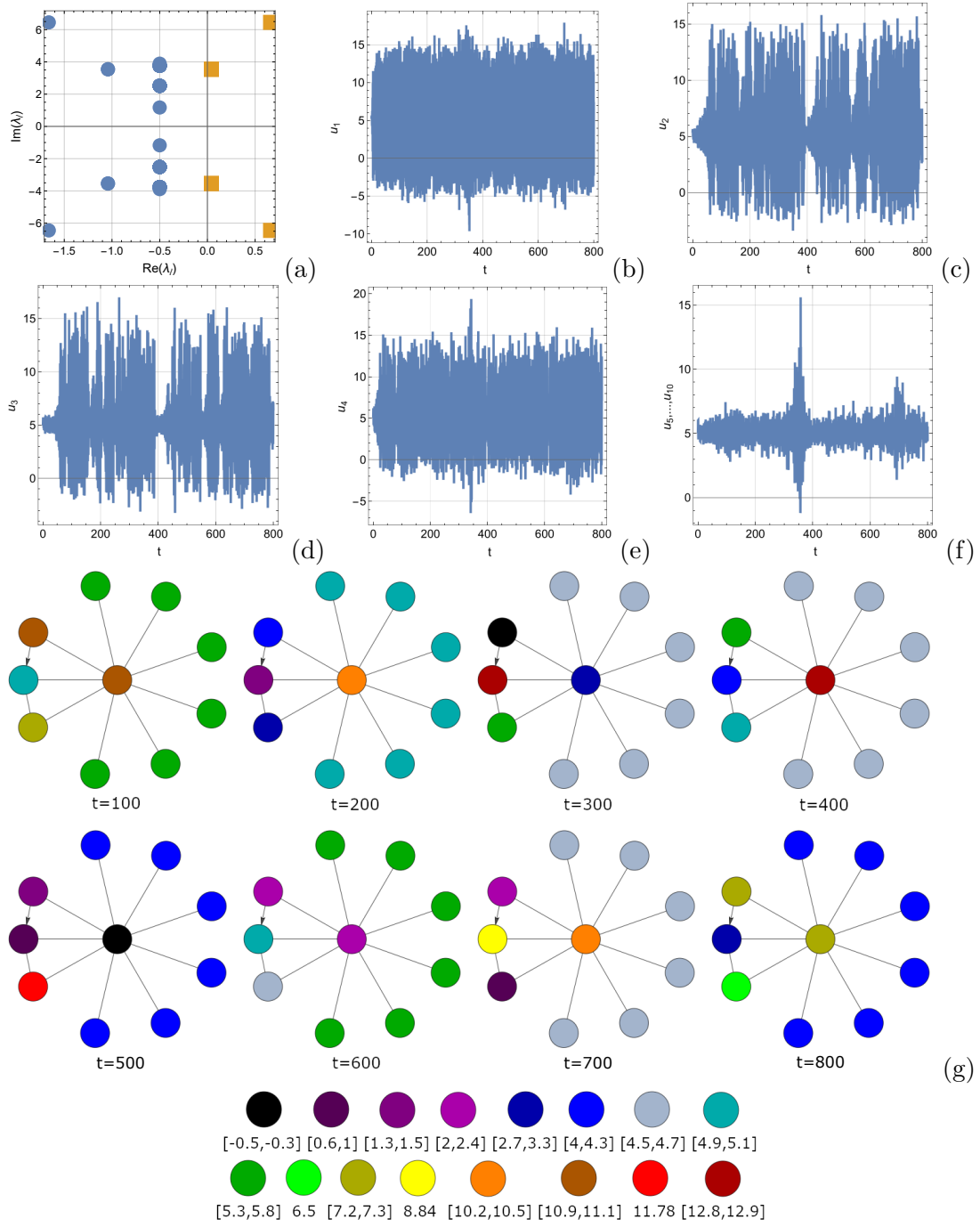


Figure 3: Patterning corresponding to the adjacency matrix Eq. (3.9). In (a) we plot the eigenvalues of the matrix M . In (b),(c),(d) and (e) we plot u_1, u_2, u_3 , and u_4 respectively, and, in (f), we plot u_5, \dots, u_{10} . Finally, in (g) we give the pattern for the function u at $t = 100, 200, 300, 400, 500, 600, 700, 800$.

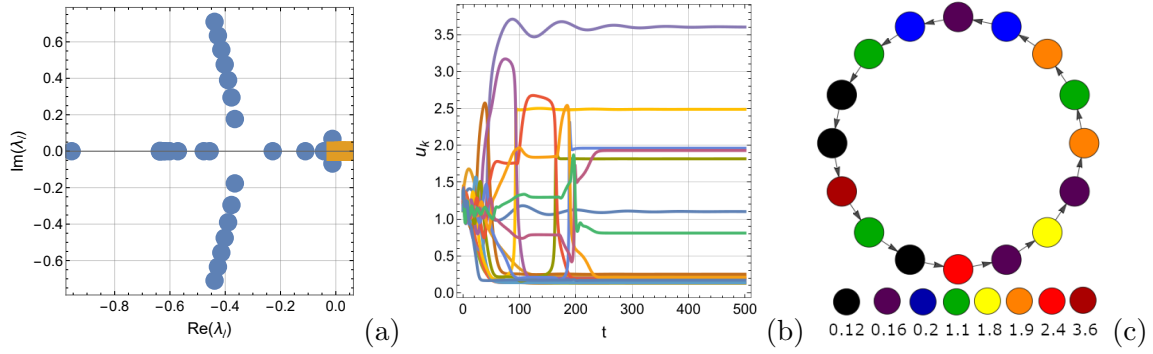


Figure 4: Patterning corresponding to the adjacency matrix Eq. (3.6) with $a_1 = 0, a_2 = 1$, and where the constants $\alpha_i, i = 1, \dots, 16$ are given by Eq. (3.14). In (a) we give the eigenvalues of the matrix M . In (b) we show the behaviour of the function u , for each of the nodes. Finally, in (c) we give the pattern for the function u at $t = 500$.

for different reaction rates at each node i.e., different β_i 's. In this subsection here we assume that the adjacency matrix A_{ij} is given by Eq. (3.6). Moreover, in this subsection we restrict ourselves to $n = 16$ nodes. Finally, it is worth noting here that one can apply the analysis presented in [24] only in the special case $\beta_i = 1$ (provided the underlying network is diagonalizable).

Let us now consider two specific choices of the constants β_i with $i = 1, \dots, n$. We first consider the choice

$$\beta_i = \frac{i}{n} = \frac{i}{16}, \quad (3.14)$$

where we have used that $n = 16$. The numerical results corresponding to Eq. (3.14) are shown in Fig. 4 for the choices $a_1 = a_2 = 0$. For these values of a_1 and a_2 the adjacency matrix Eq. (3.6) describes an incomplete cycle graph. In Fig. 4(a) we give the eigenvalues of the matrix M . In this case there are four eigenvalues with positive real part. In particular, we find that $\text{Re}(\lambda_\ell) = 0.04 > 0$ and hence we detect an instability. Here, we see that, for the choices we have made, the system Eqs. (3.12)–(3.13) generates a patterned state. This is confirmed in Fig. 4(b), where we see that the functions u_i form a stable pattern at around $t \approx 45$. The resulting pattern is shown in Fig. 4(c). It is interesting to compare Fig. 4 to the second row (plots (d)–(f)) of Fig. 2, where we found that a pattern did not emerge. This tells us that the pattern shown in Fig. 4 is purely a consequence of the global reaction kinetics.

Let us now consider a different choice of the constants $\beta_i, i = 1, \dots, 16$. In particular we consider the choice

$$\beta_i = \begin{cases} 1, & \text{if } i = 1, \\ 0, & \text{otherwise.} \end{cases} \quad (3.15)$$

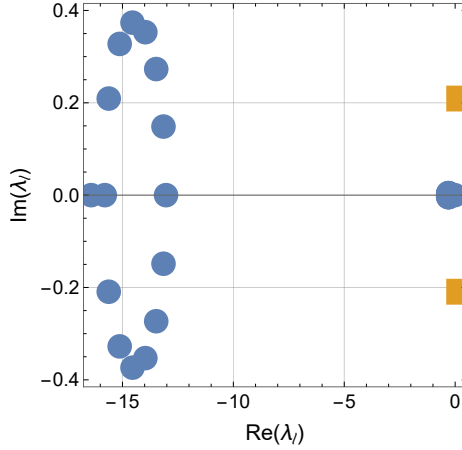


Figure 5: The eigenvalues of the matrix M corresponding to the adjacency matrix Eq. (3.6) with $a_1 = 0, a_2 = 1$, and where the constants $\alpha_i, i = 1, \dots, 16$ are given by Eq. (3.15).

Here, the reaction kinetics are non-zero at node-1 only, with no interaction between the species u_i and v_i occurring at any of the other nodes. The eigenvalues of the matrix M corresponding to Eq. (3.15) are shown in Fig. 5 for the choices $a_1 = 0$ and $a_2 = 1$. Here, there are two eigenvalues (one conjugate pair) with positive real part $\text{Re}(\lambda_\ell) = 0.17 > 0$. In this case the underlying network is a complete cycle graph. In Fig. 5 we see that the matrix M has two eigenvalues with positive real parts. Interestingly, both of these eigenvalues also have a non-zero real part, in fact the two eigenvalues are conjugate pairs. Recall that if the dominant eigenvalue (i.e., the eigenvalue with the largest real part) has a non-zero imaginary part then it is indicative of *Turing-wave instability*. This means that we do not expect the unknowns to approach a time independent solution.

This behaviour is numerically confirmed in Fig. 6, where we see that the functions u_i , for $i = 1, \dots, 16$, approach limit-cycles. In Fig. 6 we see that the values of u_i at each node naturally separate into three groups. The first of these groups contains only u_1 and is shown in Fig. 6(a). Here we see that u_1 takes the most extreme values but nevertheless approaches a stable limit-cycle at around $t \approx 300$. In Fig. 6(b) we show the second grouping, which consists of u_2 and u_{16} . Similarly, the third group is shown in Fig. 6(c), and consists of u_3-u_{15} . Note that while group two and three appear to oscillate at the same frequency, they have different amplitudes. As with group one, both groups two and three approach a stable limit-cycle at around $t \approx 300$. We show one full period of the limit cycle in Fig. 6(d), at four moments of time. It is interesting to compare this Turing-wave instability to the one shown in Fig. 3. In Fig. 6 we clearly see that the unknown approaches a stable limit cycle. Conversely, in Fig. 3 we see that although u_i appears to remain bounded its behaviour is somewhat more chaotic, and as such it is unclear whether or not the resulting behaviour describes a stable limit cycle.

Let us now end this subsection by discussing the effect of global reaction kinetics. One

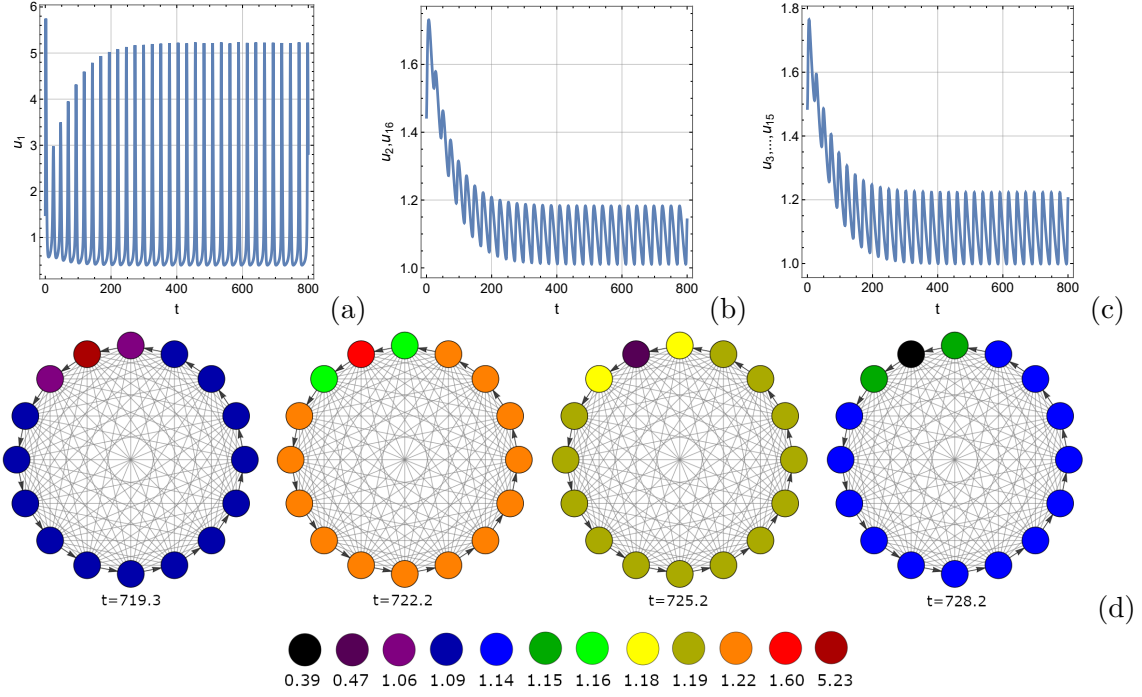


Figure 6: Patterning corresponding to the adjacency matrix Eq. (3.6) with $a_1 = 0, a_2 = 1$, and where the constants $\beta_i, i = 1, \dots, 16$ are given by Eq. (3.15). In (a) we plot the function u_1 , in (b) we plot the functions u_2 and u_{16} , and in (c) we plot the values of the function u at $t = 719.2, 722.2, 725.2, 728.2$.

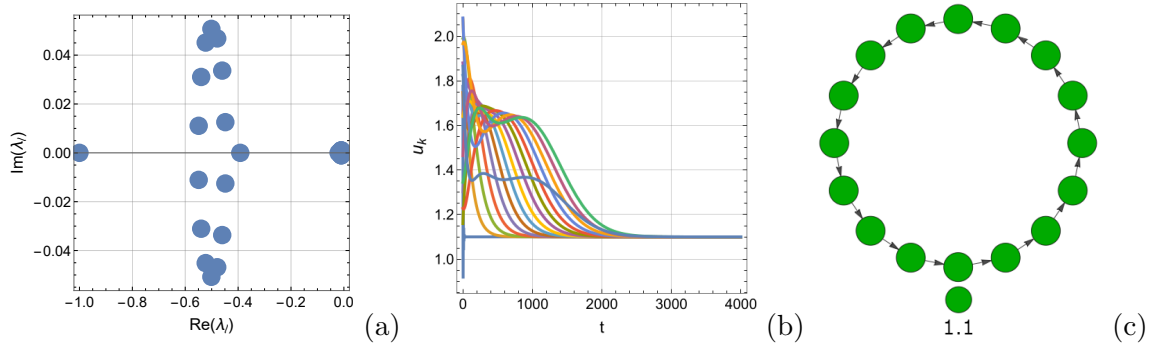


Figure 7: Lack of patterning corresponding to the adjacency matrix Eq. (3.6) with $a_1 = a_2 = 0$, and where the constants $\alpha_i, i = 1, \dots, 16$ are given by Eq. (3.15). In (a) we give the eigenvalues of the matrix M . In (b) we show the behaviour of the function u , for each of the nodes. Finally, in (c) we give show the lack of a pattern for the function u at $t = 4000$.

may be tempted to take the perspective that global reaction kinetics generically lead to patterning. From this perspective one argues that if the unknowns interact differently

at each of the nodes then one would also expect their final values to vary from node to node. Although there is some merit to this argument it is worth noting that the underlying topology of the graph can still have a significant effect on the formation of patterning. To demonstrate this we once again pick the constants $\beta_i, i = 1, \dots, n$ as in Eq. (3.15). Furthermore, we suppose the adjacency matrix A_{ij} describes an incomplete cycle graph (which corresponds to the choices $a_1 = a_2 = 0$). The numerical results for these choices are shown in Fig. 7. In Fig. 7(a) we show the eigenvalues of the matrix M . Here we see that our linear theory does *not* predict patterning, with $\text{Re}(\lambda_\ell) = -0.01 < 0$. Consistent with this we see that u_i , shown in Fig. 7(b), exhibits non-trivial behaviour for a short time only before approaching the steady state solution at around $t \approx 2200$. In Fig. 7(c) we show the values of u on each node at $t = 4000$. This example shows that even though global reaction kinetics can allow a large class of equations to generate patterns, the underlying topology nevertheless has a significant effect on the emergence of a pattern.

4 Numerical examples of pattern formation of temporal directed networks

We now consider examples of pattern formation on directed temporal networks. The goal of this section is to provide examples of the various types on non-autonomous reaction diffusion equations that can lead to pattern formation. In this section, as in Section 3, we consider only two types of networks. We once again emphasise that many of the results we present here can be applied to other types of networks. However, we find that the ones considered here are sufficient for our purposes.

4.1 Numerical methods

The numerical methods we employ here, when solving equations of the form Eq. (2.35), are largely the same as in Section 3.1. In addition to numerically solving systems of the form Eq. (2.35), we also solve the corresponding linearized system Eq. (2.36). Recall that $U_{\alpha,i}$ is the unknown of the linear system Eq. (2.36). In regards to initial data we set $U_{\alpha,i}(0) = \xi_{\alpha,i}$, where $\xi_{\alpha,i}$ is a random real number which we calculate using the Mathematica function *RandomReal[1]*. In order to present our numerical results it is useful to now introduce the following quantity:

$$w = \max_i \{\|\mathbf{U}_1\|, \dots, \|\mathbf{U}_n\|\}, \quad \|\mathbf{U}_k\| = \left(\sum_{\beta=1}^m U_{\beta,k}^2 \right)^{1/2}. \quad (4.1)$$

If there is an instability, then one expects that $w \rightarrow \infty$ as $t \rightarrow \infty$. Conversely, if the steady state is linearly stable then $w \rightarrow 0$ as $t \rightarrow \infty$. Finally, for later convenience, we define the function $\Omega(t, \eta) : \mathbb{R}^2 \rightarrow \mathbb{R}$ as

$$\Omega(t, \eta) = \frac{1}{2} \tanh \left(\frac{1}{10} (t - \eta) \right). \quad (4.2)$$

In this section here we use $\Omega(t, \eta)$ as a smooth switch function, where $t = \eta$ is the “switch point”.

4.2 Pattern formation on directed temporal networks

For our first example, of pattern formation on a directed temporal networks, we consider the following system:

$$\frac{du_i}{dt} = \frac{1}{50} \sum_{j=1}^n A_{ij}(t) (u_j - u_i) + \beta_i(t) \left(\frac{1}{10} - u_i + u_i^2 v_i \right), \quad (4.3)$$

$$\frac{dv_i}{dt} = \sum_{j=1}^n A_{ij}(t) (v_j - v_i) + \beta_i(t) (1 - u_i^2 v_i), \quad (4.4)$$

for freely specifiable functions $\beta_i : \mathbb{R} \rightarrow \mathbb{R}$, with $i = 1, \dots, n$. The adjacency matrix A_{ij} is

$$A_{ij} = \begin{cases} 1/2 & \text{if } i - j = 1 \text{ or } i - j = n - 1, \\ 0 & \text{if } i - j = 0 \\ h(t) & \text{otherwise,} \end{cases} \quad (4.5)$$

where $h(t)$ is also a freely specifiable function. In this example here we set $h(t) = 1 - \Omega(t, 200) + \Omega(t, 300)$, and $\beta_i(t) = 1$ for all $i = 1, \dots, n$ with $n = 16$. Notice that, for $\beta_i(t) = 1$, Eqs. (4.3) and (4.4) have local reaction kinetics that do not depend on time. However, the network itself *does* change in time. The function $h(t)$ is shown in Fig. 8(a). In Fig. 8(a) we see that $h(t) \approx 1$ if $t < 200$ or $t > 300$, and therefore describes a complete cycle graph in these regions. However, for $t \in (200, 300)$ we have that $h(t) \approx 0$, in which case the adjacency matrix Eq. (4.5) corresponds to an *incomplete* cycle graph.

In Fig. 8 we show the numerical results corresponding to this network. In Fig. 8(b) we show the numerically calculated quantity $\ln(w)$. Here, we see that w clearly grows for $t < 200$ and $t > 300$, indicating an instability in these regions. Conversely, for $t \in (200, 300)$, we see that w is *decreasing*. We therefore conclude that the steady state solution $(u_i, v_i) = (11/10, 100/121)$ is linearly stable in this region (and therefore does not produce a pattern). This behaviour is verified in Fig. 8(c), where we see that a pattern occurs for $t < 200$ and $t > 300$, but is suppressed for $t \in (200, 300)$. This result is not surprising as network topology is known to significantly effect patterning (see, for example, [18, 19, 35]).

4.3 Pattern formation with time dependent reaction kinetics

In addition to being able to control the topology, the theory presented in Section 2.3 also allows one to investigate non-autonomous reaction diffusion equations on *static* networks. In this subsection here we first consider systems with time dependent reaction kinetics. To this end, we again consider Eqs. (4.3)–(4.4). Here, we consider two different choices of the adjacency matrix A_{ij} .

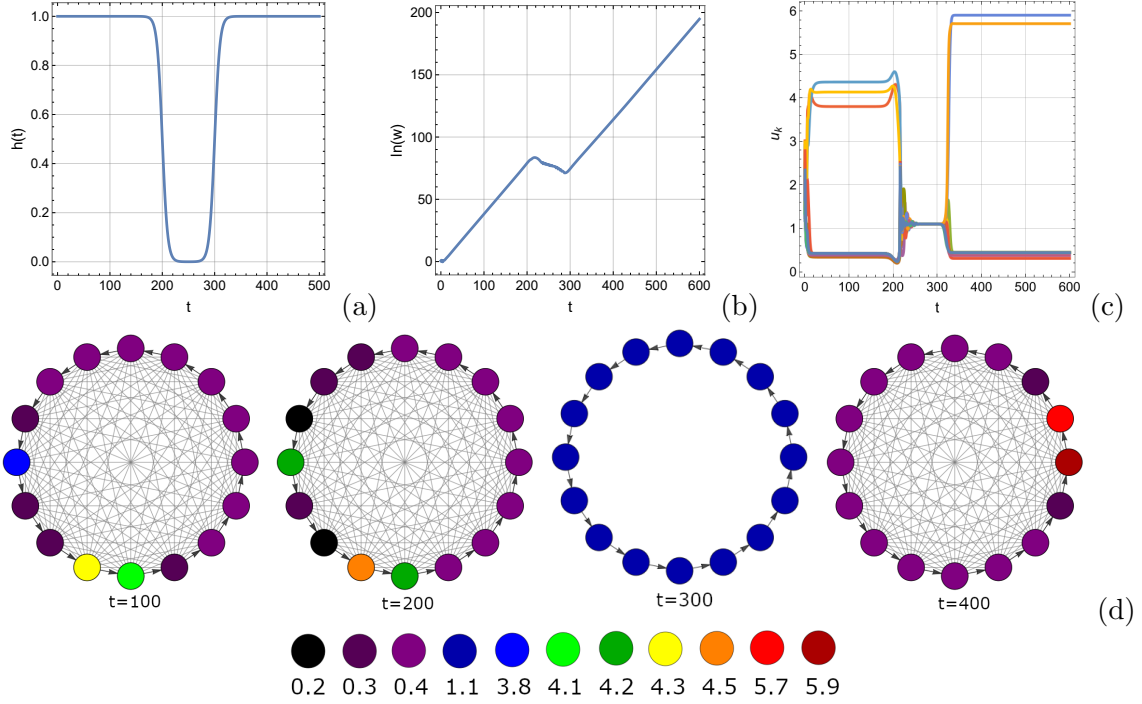


Figure 8: Patterning corresponding to Eqs. (4.3)–(4.5) with $h(t) = 1 - \Omega(t, 200) + \Omega(t, 300)$, and $\beta_i(t) = 1$. In (a) we plot the function $h(t)$. In (b) we show the quantity $\ln(w)$. In (c) we plot the functions u_i for $i = 1, \dots, 16$. Finally, in (d) we show the values of u_i on the graph at $t = 100, 200, 300, 400$.

We first suppose that $n = 10$ and that the adjacency matrix A_{ij} is given by Eq. (3.9). Recall that this choice of adjacency matrix describes a “modified star graph”. Moreover, we set $\beta_i(t) = 1 - \Omega(t, 200) + \Omega(t, 400)$ for $i = 1, \dots, 10$, so that Eqs. (4.3)–(4.4) have local reaction kinetics. A plot of $\beta_k(t)$ is shown in Fig. 9(a). In Fig. 9(a) we see that $\beta_k(t) \approx 1$ if $t < 200$ or $t > 400$. Conversely, for $t \in (200, 400)$ we see that $\beta_k(t) \approx 0$. This has the effect of turning the reaction kinetics “off” for $t \in (200, 400)$ and we would therefore not expect a pattern to occur in this region. The corresponding numerical results are shown in Fig. 9. In Fig. 9(b) we show the numerically calculated quantity $\ln(w)$. Here, we see that w clearly grows for $t < 200$ and $t > 400$, indicating an instability in these regions. Conversely, for $t \in (200, 400)$, we see that w is *decreasing*. We therefore conclude that the steady state solution $(u_i, v_i) = (11/10, 100/121)$ is linearly stable in this region (and therefore does not produce a pattern). This behaviour is verified in Fig. 9(c), where we see that a pattern occurs for $t < 200$ and $t > 400$, but is suppressed for $t \in (200, 400)$. The corresponding pattern is shown in Fig. 9(d) at four time points.

We now consider examples of pattern formation with global reaction kinetics. For this we again consider Eqs. (4.3)–(4.4), where the adjacency matrix A_{ij} is given by Eq. (4.5) with $n = 2$. We now consider two choices of the functions $h(t)$ and $\beta_i(t)$.

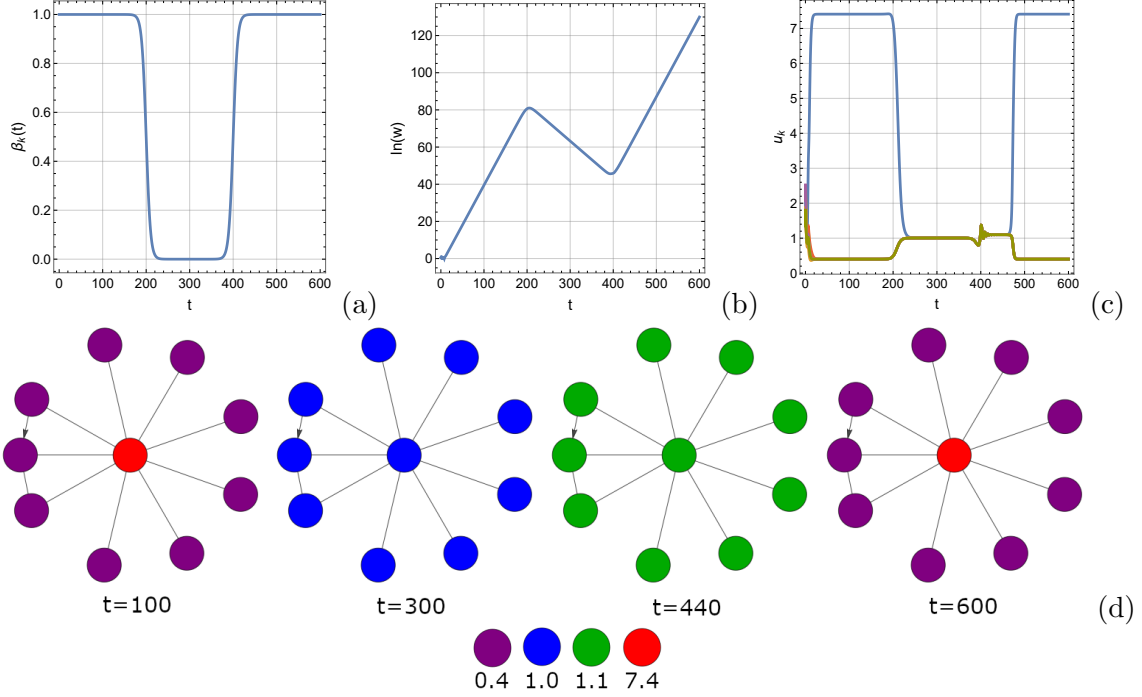


Figure 9: Patterning corresponding to Eqs. (4.3)–(4.4) with A_{ij} given by Eq. (3.9) and $\beta_i(t) = 1 - \Omega(t, 200) + \Omega(t, 400)$ for all $i = 1, \dots, 10$. In (a) we plot the function $\beta_k(t)$. In (b) we show the quantity $\ln(w)$. In (c) we plot the functions u_i for $i = 1, \dots, 10$. Finally, in (d) we show the values of u_i on the graph at $t = 100, 300, 440, 600$.

We first set $h(t) = 0$. Recall that, for this particular choice of $h(t)$, the underlying network is an incomplete cycle graph. Moreover, we pick

$$\beta_i(t) = \frac{i}{16}r(t), \quad r(t) = \Omega(t, 2500) - \Omega(t, 4000). \quad (4.6)$$

A plot of the function $r(t)$ is shown in Fig. 10(a). In Fig. 10(a) we see that $r(t) \approx 1$ for $t \in (2500, 4000)$, and $r(t) \approx 0$ for $t \in (0, 2500) \cup (4000, \infty)$. This has the effect of “switching on” the reaction kinetics for a short while. The numerical results corresponding to these choices are shown in Fig. 10. In Fig. 10(b) we show the numerically calculated quantity $\ln(w)$. Here we see that $w \approx 0$ for $t \in (0, 2500)$, and we therefore do not expect a pattern to form in this region. However, when the kinetics are “switched on” at $t = 2500$, w quickly grows. When the reaction kinetics are again “switched off” we see that w begins to decrease toward $w \approx 0$. This behaviour is confirmed in Fig. 10(c). In Fig. 10(d) we show the patterning resulting from u_i with $i = 1, \dots, n$ at different times.

For our second example of global reaction kinetics, we set $h(t) = 1$. Recall that, for this particular choice of $h(t)$, the underlying network is a complete cycle graph. Moreover, we

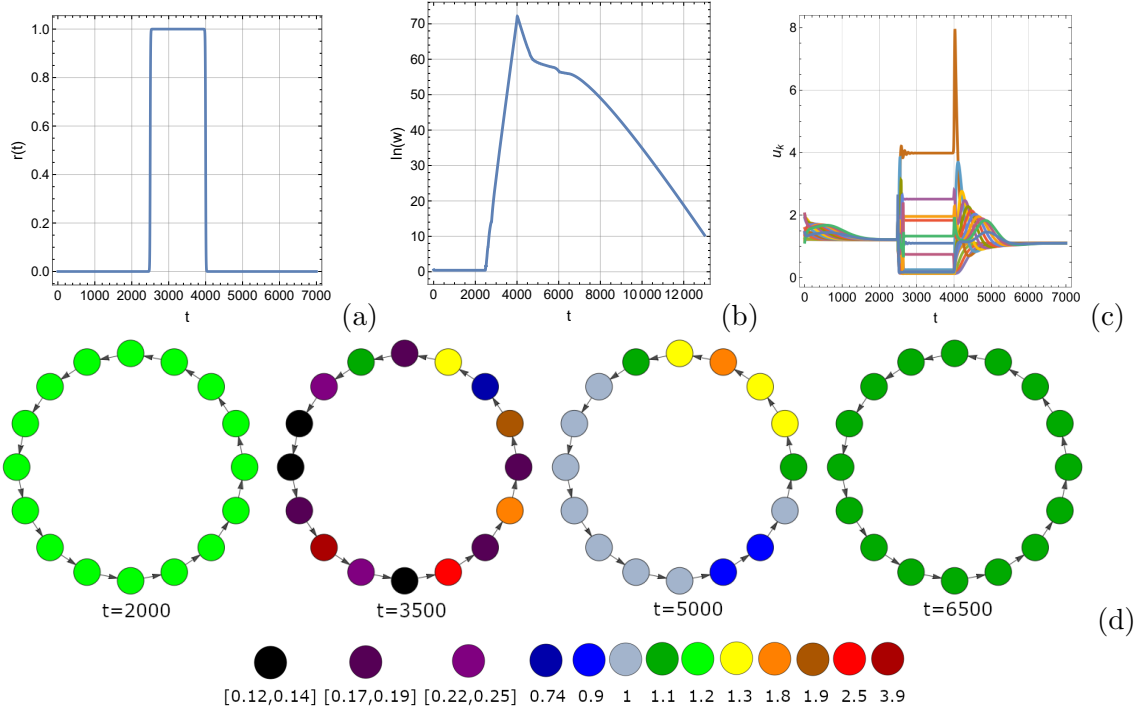


Figure 10: Patterning corresponding to Eqs. (4.3)–(4.5) with $h(t) = 0$, and where $\beta_i(t)$ is given by Eq. (4.6) for $i = 1, \dots, n = 16$. In (a) we plot the function $h(t)$. In (b) we show the numerically calculated quantity $\ln(w)$. In (c) we plot the functions u_i for $i = 1, \dots, 16$. Finally, in (d) we show the values of u_i on the graph at $t = 297, 3500, 5000, 6500$.

set

$$\beta_i(t) = \begin{cases} 1, & \text{if } i = 1, \\ 1/2 - \Omega(t, 200), & \text{otherwise.} \end{cases} \quad (4.7)$$

A plot of the function $1/2 - \Omega(t, 200)$ is given in Fig. 11(a). In Fig. 11(a) we see that $1/2 - \Omega(t, 200) \approx 1$ for $t \in (0, 200)$, and $1/2 - \Omega(t, 200) \approx 0$ for $t > 200$. When $t < 200$ the unknowns are allowed to interact at all of the nodes. In fact, for this region, the reaction kinetics are *local*, not global. However, for $t > 200$ the reactions become zero at all nodes, excluding node 1. In this region the reaction kinetics are global. This is therefore an example that begins with local reaction kinetics that evolve into global ones.

The numerical results corresponding to these choices are shown in Fig. 11. In Fig. 11(b) we show the numerically calculated quantity $\ln(w)$. For $t < 200$ we see that w is an increasing function. This suggests that a stable pattern forms, at least while $t < 200$. This behaviour changes when the reaction kinetics become global, which occurs for $t > 200$. Here, we find that the quantity w continues to grow. However, in addition to growth we can also clearly see small oscillations. These oscillations are also shown in Fig. 11(c). We

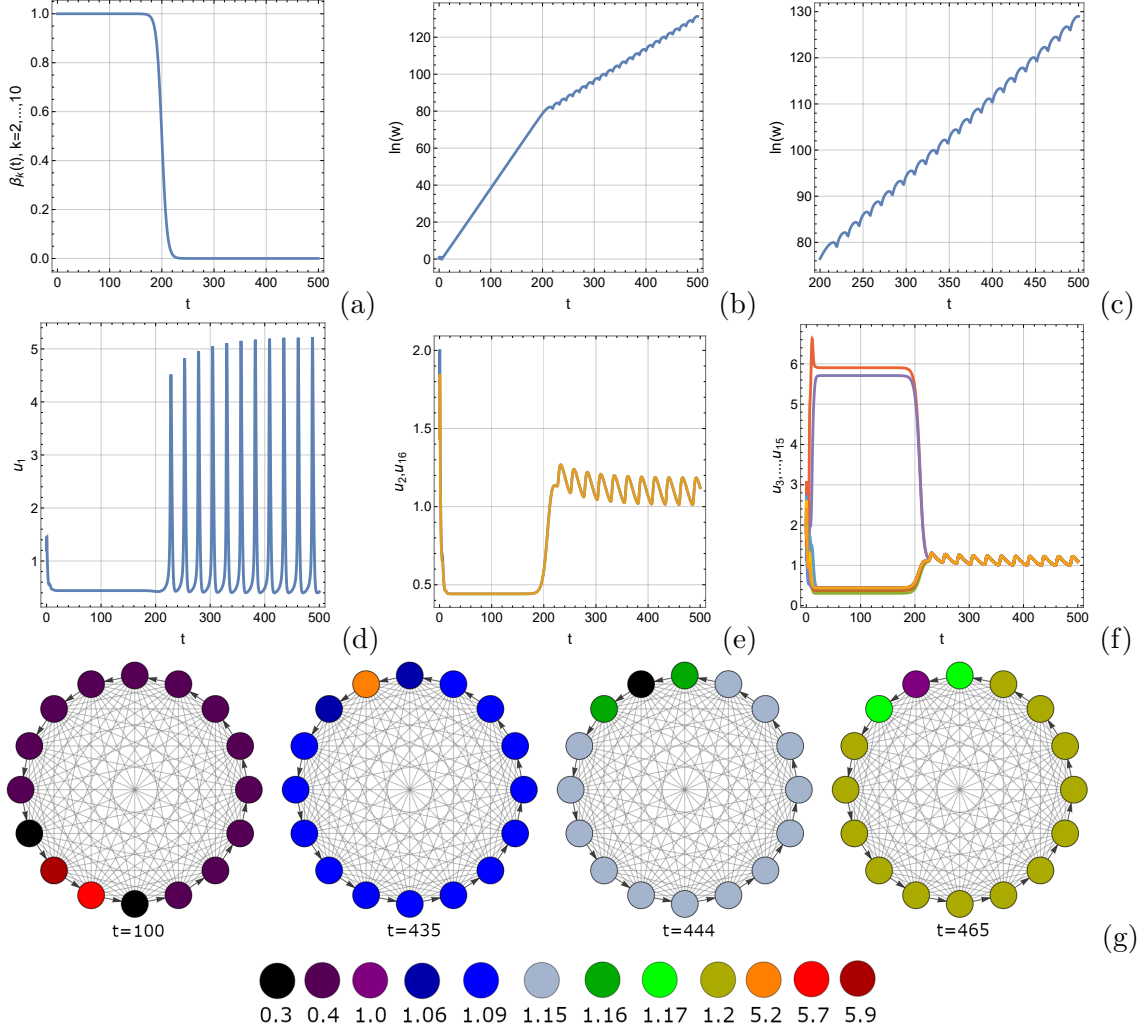


Figure 11: Patterning corresponding to Eqs. (4.3)–(4.5) with $h(t) = 1$, and where $\beta_i(t)$ is given by Eq. (4.7) for $i = 1, \dots, n = 16$. In (a) we plot the function $1/2 - \Omega(t, 200)$. In (b) we show the numerically calculated quantity $\ln(w)$. In (d) we plot the function u_1 , in (e) we plot the functions u_2 and u_{16} , and in (f) we show the functions u_3 – u_{15} . Finally, in (g) we show the values of u_i on the graph at $t = 100, 435, 444, 465$.

interpret this as follows: For $t > 200$ the system experiences a *Turning-wave* instability. Exactly this behaviour is shown in Fig. 11(d)–(f). Here, as in Section 3.5, we find that the values of u_i naturally split into three groups based on how they oscillate. The first group contains u_1 only and is shown in Fig. 11(d). In Fig. 11(e) we show the second group, which consist of u_2 and u_{16} . In Fig. 11(f) we show the third group, which contains u_3 – u_{15} . Finally, in (g) we show the values of u_i on the graph at $t = 100, 435, 444, 465$.

4.4 Pattern formation with time-dependent diffusion coefficients

Another way in which non-autonomous reaction diffusion equations can occur, is if the diffusion coefficients themselves depend on time. The purpose of this subsection here is to provide one such example. To this end we consider the *hyperbolic reaction-diffusion* system

$$\frac{d^2 u_i}{dt^2} + \frac{du_i}{dt} = d(t) \sum_{j=1}^{10} A_{ij} (u_j - u_i) + 5 - 10u_i + u_i^2 v_i, \quad (4.8)$$

$$\frac{d^2 v_i}{dt^2} + \frac{dv_i}{dt} = \sum_{j=1}^{10} A_{ij} (v_j - v_i) + 9u_i - u_i^2 v_i, \quad (4.9)$$

where A_{ij} is given by Eq. (3.9), and $d(t) = 149(1 + 2\Omega(t, 300))/100$. Recall again that this particular choice of adjacency matrix describes a “modified star graph”. A plot of the diffusion coefficient $d(t)$ is shown in Fig. 12(a). For $t \in (0, 300)$ we have that $d \approx 1/50$, and for $t > 300$ we have that $d(t) \approx 3$. The numerical results for this system are shown in Fig. 12. In Fig. 12(b) we show the numerically calculated quantity $\ln(w)$. Here we see that w is increasing on the entire numerical domain and hence we expect a pattern to form for all $t \in (0, 700)$. For $t < 300$, w increases linearly. Conversely, for $t > 300$ the function w oscillates as it increases. These oscillations are shown in Fig. 12(c). This tells us that the system experiences a Turing instability for $t < 300$ and a *Turing-wave* instability for $t > 300$. This behaviour is shown in Fig. 11(d). Here, as in Section 3.4, we find that the values of u_i naturally split into five groups based on how they oscillate. The first four groups contain one element only. Namely, u_1, u_2, u_3 and u_4 . Each of these functions are shown in Fig. 11(e), Fig. 11(f), Fig. 11(g), and Fig. 11(h), respectively. In Fig. 11(i) we show the fifth group, which consists of $u_2 - u_{10}$. Finally, in (j) we show the values of u_i on the graph at $t = 200, 400, 500, 600$.

5 Conclusions

In this work we have established a method for determining instability, leading to pattern formation, on directed networks. We started by investigating systems of autonomous reaction-diffusion equations on static networks. One of our primary focuses here was to establish a method for determining instability (leading to pattern formation) on non-diagonalizable networks. That is, networks whose Laplacian matrix is non-diagonalizable. In this setting, the eigenvectors of the Laplacian matrix do not form a complete orthonormal basis over the network. Thus, in order to perform an instability analysis, we first had to pick a basis. To do this we symmetrized the adjacency matrix. In doing so we are able to express our original system as the equivalent problem of solving a system of reaction-diffusion equations on an *undirected network* with *global reaction kinetics*. The basis was then constructed as the eigenvectors of the ‘symmetrized Laplacian’, i.e., the Laplacian calculated from the symmetrized adjacency matrix. We were able to show that this approach reduces

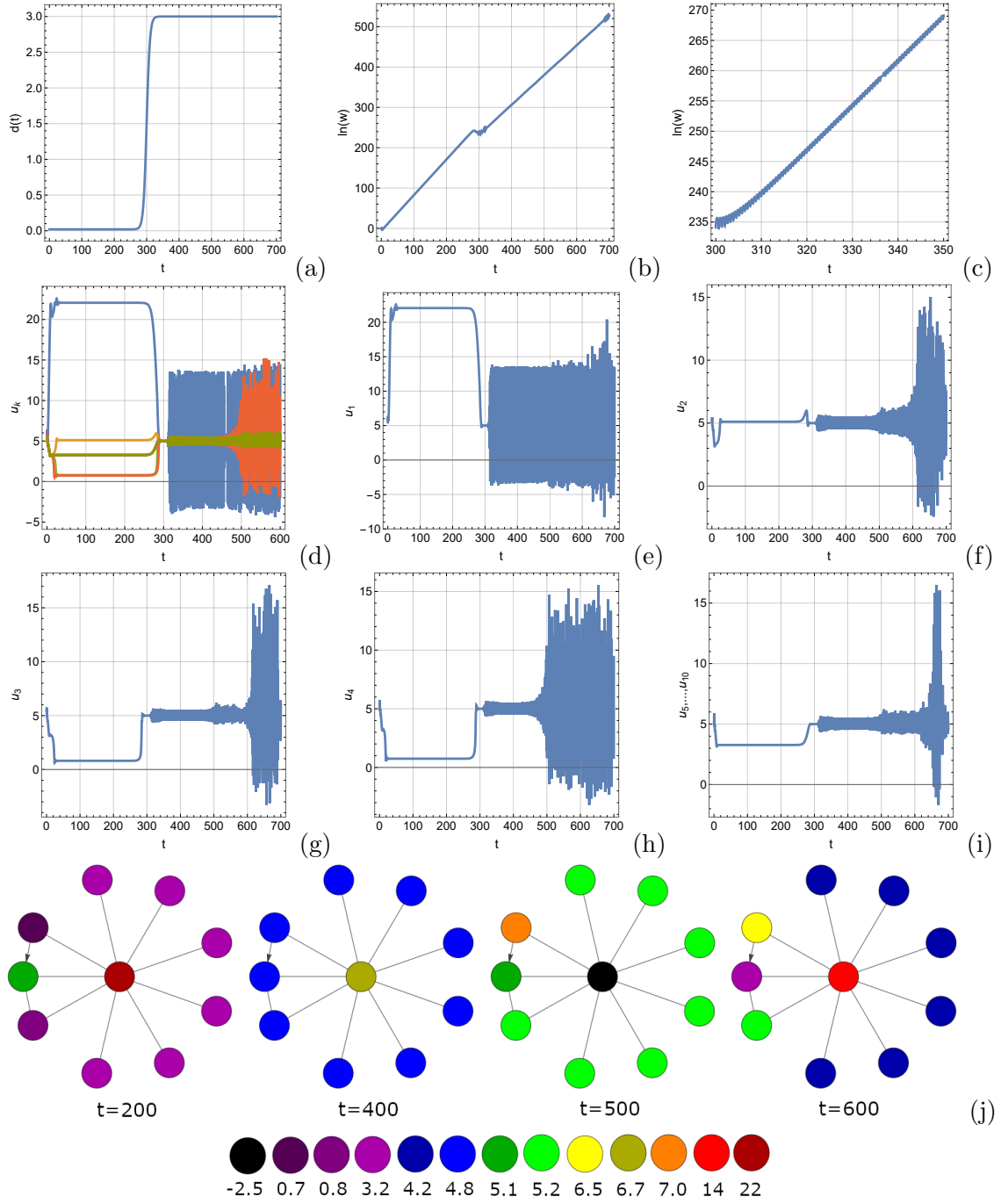


Figure 12: Patterning corresponding Eqs. (4.8) and (4.9) with A given by Eq. (3.9). In (a) we plot the diffusion coefficient $d(t)$. In (b) and (c) we show $\ln(w)$. In (d) we plot the functions u_k and in plots (e)–(h) we plot u_1, u_2, u_3 , and u_4 respectively, and, in (i), we plot u_5, \dots, u_{10} . Finally, in (j) we give the pattern for the functions u_k at $t = 200, 400, 500, 600$.

to the standard Turing analysis in the case of autonomous reaction-diffusion equations on undirected networks with local reaction-kinetics. In addition to static non-diagonalizable networks we also discussed *global reaction kinetics*. This line of investigation rose naturally from our method for constructing a basis. Here we found that global reaction kinetics allowed for Turing-pattern formation to occur on networks that did *not* allow for patterning from reaction-diffusion equations with local reaction kinetics. The approach that we use here has the drawback that our instability condition must be implemented numerically. However, our instability condition can nevertheless be applied to a large class of reaction-diffusion equations on simple networks, without any restrictions on the network structure. In future works it would be interesting to extend our approach here to more complicated networks, such as multiplex networks (see, for example, [12]).

In addition to this we also investigated pattern formation arising from non-autonomous reaction-diffusion equations on *temporal* networks. That is, networks that are allowed to change in time. Our primary focus here was to once again establish a method to determine instability (leading to pattern formation) on temporal networks. In order to determine linear instability we studied the linearized equations (corresponding to the original system) directly, without any basis decompositions. This approach required us to numerically solve linearized equations. This raises the question *why not solve the original, non-linear, system instead?* After all, in either setting one must solve a system of ODE's. One could certainly do this, however, it is worth noting that it is, in general, less computational expensive to solve a system of m -linear equations, on an n -node network, than a system of m -non-linear equations. Moreover, this approach is useful if one wants to find what system parameters lead to a Turing-instability. As it is less time consuming to run multiple simulations of the linearized system, than it is to run multiple simulations of the linearized system.

References

- [1] Turing, A.M. The chemical basis of morphogenesis. *Philosophical Transactions of the Royal Society of London. B*, 237, 1952. DOI: [10.1098/rstb.1952.0012](https://doi.org/10.1098/rstb.1952.0012).
- [2] Tompkins, N. and Li, N. and Girabawe, C. and Heymann, M. and Ermentrout, G.B. and Epstein, I. and Fraden, S. Testing Turing’s theory of morphogenesis in chemical cells. *PNAS*, 111, 2014. DOI: [10.1073/pnas.1322005111](https://doi.org/10.1073/pnas.1322005111).
- [3] Ouyang, Q. and Swinney, H.L. Transition from a uniform state to hexagonal and striped turing patterns. *Nature*, 352, 1991. DOI: [10.1038/352610a0](https://doi.org/10.1038/352610a0).
- [4] Lengyel, I. and Epstein, I.R. A chemical approach to designing Turing patterns in reaction-diffusion systems. *Proceedings of the National Academy of Sciences*, 89, 1992. DOI: [10.1073/pnas.89.9.3977](https://doi.org/10.1073/pnas.89.9.3977).
- [5] Maini, P. and Baker, R.E. and Chuong, C.M. The turing model comes of molecular age. *Science*, 314, 2006. DOI: [10.1126/science.1136396](https://doi.org/10.1126/science.1136396).
- [6] Seul, M. and Andelman, D. Domain shapes and patterns: the phenomenology of modulated phases. *Science*, 267, 1995. DOI: [10.1126/science.267.5197.476](https://doi.org/10.1126/science.267.5197.476).
- [7] Maini, P. and Painter, K. and Chau, H. Spatial pattern formation in chemical and biological systems. *Journal of the Chemical Society, Faraday Transactions*, 93, 1997. DOI: [10.1039/A702602A](https://doi.org/10.1039/A702602A).
- [8] Baker, R.E and Gaffney, E.A. and Maini, P.K. Partial differential equations for self-organization in cellular and developmental biology. *Nonlinearity*, 21, 2008. DOI: [10.1088/0951-7715/21/11/R05](https://doi.org/10.1088/0951-7715/21/11/R05).
- [9] Marcon, L. and Sharpe, J. Turing patterns in development: what about the horse part? *Current Opinion in Genetics & Development*, 22, 2012. DOI: [10.1016/j.gde.2012.11.013](https://doi.org/10.1016/j.gde.2012.11.013).
- [10] Van Gorder, R.A. Influence of temperature on Turing pattern formation. *Proceedings of the Royal Society A*, 476, 2020. DOI: [10.1098/rspa.2020.0356](https://doi.org/10.1098/rspa.2020.0356).
- [11] Kouvaris, N.E. and Hata, S. and Díaz-Guilera, A. Pattern formation in multiplex networks. *Scientific Reports*, 5, 2015. DOI: [10.1038/srep10840](https://doi.org/10.1038/srep10840).
- [12] Asllani, M. and Busiello, D. M. and Carletti, T. and Fanelli, D. and Planchon, G. Turing patterns in multiplex networks. *Phys. Rev. E*, 90, 2014. DOI: [10.1103/PhysRevE.90.042814](https://doi.org/10.1103/PhysRevE.90.042814).
- [13] Ermentrout, B. Neural networks as spatio-temporal pattern-forming systems. *Reports on Progress in Physics*, 61, 1998. DOI: [10.1088/0034-4885/61/4/002](https://doi.org/10.1088/0034-4885/61/4/002).

- [14] Pastor-Satorras, R. and Vespignani, A. Complex networks: patterns of complexity. *Nature Physics*, 6, 2010. DOI: [10.1038/nphys1722](https://doi.org/10.1038/nphys1722).
- [15] Padirac, A. and Fujii, T. and Estévez-Torres, A. and Rondelez, Y. Spatial waves in synthetic biochemical networks. *Journal of the American Chemical Society*, 135, 2013. DOI: [10.1021/ja403584p](https://doi.org/10.1021/ja403584p).
- [16] Kouvaris, N.E. and Sebek, M. and Mikhailov, A.S. and Kiss, I.Z. Self-organized stationary patterns in networks of bistable chemical reactions. *Angewandte Chemie*, 128, 2016. DOI: [10.1002/ange.201607030](https://doi.org/10.1002/ange.201607030).
- [17] McCullen, N. and Wagenknecht, T. Pattern formation on networks: from localised activity to Turing patterns. *Scientific reports*, 6, 2016. DOI: [10.1038/srep27397](https://doi.org/10.1038/srep27397).
- [18] Mimar, S. and Juane, M.M. and Park, J. and Munuzuri, A.P. and Ghoshal, G. Turing patterns mediated by network topology in homogeneous active systems. *Physical Review E*, 99, 2019. DOI: [10.1103/PhysRevE.99.062303](https://doi.org/10.1103/PhysRevE.99.062303).
- [19] Asllani, M. and Carletti, T. and Fanelli, D. Tune the topology to create or destroy patterns. *The European Physical Journal B*, 89, 2016. DOI: [10.1140/epjb/e2016-70248-6](https://doi.org/10.1140/epjb/e2016-70248-6).
- [20] Di Patti, F. and Fanelli, D. and Miele, F. and Carletti, T. Benjamin–Feir instabilities on directed networks. *Chaos, Solitons, & Fractals*, 96, 2017. DOI: [10.1016/j.chaos.2016.11.018](https://doi.org/10.1016/j.chaos.2016.11.018).
- [21] Dhingra, N.K. and Colombino, M. and Jovanović, M.R. Structured Decentralized Control of Positive Systems With Applications to Combination Drug Therapy and Leader Selection in Directed Networks. *IEEE Transactions on Control of Network Systems*, 6, 2019. DOI: [10.1109/TCNS.2018.2820499](https://doi.org/10.1109/TCNS.2018.2820499).
- [22] Park, S.M. and Kim, B.J. Dynamic behaviors in directed networks. *Physical Review E*, 74, 2006. DOI: [10.1103/PhysRevE.74.026114](https://doi.org/10.1103/PhysRevE.74.026114).
- [23] Son, S.W. and Christensen, C. and Bizhani, G. and Foster, D.V. and Grassberger, P. and Paczuski, M. Sampling properties of directed networks. *Physical Review E*, 86, 2012. DOI: [10.1103/PhysRevE.86.046104](https://doi.org/10.1103/PhysRevE.86.046104).
- [24] Asllani, M. Challenger, J.D. Pavone, F.S. Sacconi, L. Fanelli D. The theory of pattern formation on directed networks. *Nature communications* 5, 2014. DOI: [10.1038/ncomms5517](https://doi.org/10.1038/ncomms5517).
- [25] Blanchini, F. and Casagrande, D. and Giordano, G. and Viaro, U. A Bounded Complementary Sensitivity Function Ensures Topology-Independent Stability of Homogeneous Dynamical Networks. *IEEE Transactions on Automatic Control*, 63, 2018. DOI: [10.1109/TAC.2017.2737818](https://doi.org/10.1109/TAC.2017.2737818).

- [26] Wu, M. A note on stability of linear time-varying systems. *IEEE Transactions on Automatic Control*, 19, 1974. DOI: [10.1109/TAC.1974.1100529](https://doi.org/10.1109/TAC.1974.1100529).
- [27] Knobloch, E. and Merryfield, W. Enhancement of diffusive transport in oscillatory flows. *Astrophysical Journal*, 401, 1992. DOI: [10.1086/172052](https://doi.org/10.1086/172052).
- [28] Josić, K. and Rosenbaum, R. Unstable solutions of nonautonomous linear differential equations. *SIAM Review*, 50, 2008. DOI: [10.1137/060677057](https://doi.org/10.1137/060677057).
- [29] Mierczynski, J. Instability in linear cooperative systems of ordinary differential equations. *SIAM Review*, 59, 2017. DOI: [10.1137/060677057](https://doi.org/10.1137/060677057).
- [30] Holme, P. and Saramäki, J. Temporal networks. *Physics Reports*, 519, 2012. DOI: [10.1016/j.physrep.2012.03.001](https://doi.org/10.1016/j.physrep.2012.03.001).
- [31] Ward, J.A. and Grindrod, P. Aperiodic dynamics in a deterministic adaptive network model of attitude formation in social groups. *Physica D*, 282, 2014. DOI: [10.1016/j.physd.2014.05.006](https://doi.org/10.1016/j.physd.2014.05.006).
- [32] Li, A. and Cornelius, S.P. and Liu, Y.Y. and Wang, L. and Barabási, A.L. The fundamental advantages of temporal networks. *Science*, 358, 2017. DOI: [10.1126/science.aai7488](https://doi.org/10.1126/science.aai7488).
- [33] Van Gorder, R.A. Turing and Benjamin–Feir instability mechanisms in non-autonomous systems. *Proceedings of the Royal Society A*, 476, 2020. DOI: [10.1098/rspa.2020.0003](https://doi.org/10.1098/rspa.2020.0003).
- [34] Van Gorder, R. and Klika, V. and Karuse, A.L. Turing conditions for pattern forming systems on evolving manifolds. *Journal of mathematical biology*, 2021. DOI: [10.1007/s00285-021-01552-y](https://doi.org/10.1007/s00285-021-01552-y).
- [35] Van Gorder, R.A. A theory of pattern formation for reaction-diffusion systems on temporal networks. *Proceedings of the Royal Society A*, 447, 2020. DOI: [10.1098/rspa.2020.0753](https://doi.org/10.1098/rspa.2020.0753).
- [36] Van Gorder, R.A. Pattern formation from spatially heterogeneous reaction–diffusion systems. *Philosophical Transactions of the Royal Society A*, 379, 2021. DOI: [10.1098/rsta.2021.0001](https://doi.org/10.1098/rsta.2021.0001).
- [37] Ding, Y. and Ermentrout, B. Traveling waves in non-local pulse-coupled networks. *Journal of Mathematical Biology*, 82, 2021. DOI: [10.1007/s00285-021-01572-8](https://doi.org/10.1007/s00285-021-01572-8).
- [38] Carletti, T. and Duccio, T. Pattern Formation on Hypergraphs. In *Higher-Order Systems*, pages 163–180. Springer, 2022.
- [39] Al-Ghoul, M. and Chan Eu, B. Hyperbolic reaction-diffusion equations and irreversible thermodynamics: II. Two-dimensional patterns and dissipation of energy and matter. *Physica D: Nonlinear Phenomena*, 97, 1996. DOI: [10.1016/0167-2789\(96\)00008-5](https://doi.org/10.1016/0167-2789(96)00008-5).

- [40] Zemskov, E.P. and Horsthemke, W. Diffusive instabilities in hyperbolic reaction-diffusion equations. *Physical Review E*, 93, 2016. DOI: [10.1103/PhysRevE.93.032211](https://doi.org/10.1103/PhysRevE.93.032211).
- [41] Ritchie, J.S. and Krause, A.L. and Van Gorder, R.A. Turing and wave instabilities in hyperbolic reaction-diffusion systems: The role of second-order time derivatives and cross-diffusion terms on pattern formation. *arXiv Preprint*, 2022. DOI: [arXiv.2204.13820](https://doi.org/10.1103/PhysRevE.93.032211).
- [42] Zhabotinsky, A. and Dolnik, M. and Epstein, I. Pattern formation arising from wave instability in a simple reaction-diffusion system. *The Journal of Chemical Physics*, 103:10306–10314, 1995. DOI: [10.1063/1.469932](https://doi.org/10.1063/1.469932).

Statements & Declarations

The author declares that no funds, grants, or other support were received during the preparation of this manuscript. The author has no relevant financial or non-financial interests to disclose.

Research Data Availability

Data sharing not applicable to this article as no datasets were generated or analysed during the current study.